BRAIN RESEARCH 1149 (2007) 223-231

available at www.sciencedirect.com

ScienceDirect

www.elsevier.com/locate/brainres

BRAIN RESEARCH

Research Report

Granulocyte colony-stimulating factor (G-CSF) mobilizes bone marrow-derived cells into injured spinal cord and promotes functional recovery after compression-induced spinal cord injury in mice

Masao Koda[a,*], *Yutaka Nishio*[a], *Takahito Kamada*[a], *Yukio Someya*[a], *Akihiko Okawa*[a], *Chisato Mori*[b], *Katsunori Yoshinaga*[c], *Seiji Okada*[d], *Hideshige Moriya*[a], *Masashi Yamazaki*[a]

[a]*Department of Orthopaedic Surgery, Chiba University, Graduate School of Medicine, 1-8-1 Inohana, Chuo-ku, Chiba 260-8670, Japan*
[b]*Department of Bioenvironmental Medicine, Chiba University, Graduate School of Medicine, Chiba, Japan*
[c]*Chiba Rehabilitation Center, Chiba, Japan*
[d]*Division of Hematopoiesis, Center for AIDS Research, Kumamoto University, Kumamoto, Japan*

ARTICLE INFO

Article history:
Accepted 21 February 2007
Avaialble online 1 March 2007

Keywords:
Granulocyte colony stimulating factor (G-CSF)
Spinal cord injury
Bone marrow-derived cell
Functional recovery

ABSTRACT

The aim of the present study was to elucidate the effects of granulocyte colony-stimulating factor (G-CSF)-mediated mobilization of bone marrow-derived stem cells on the injured spinal cord. Bone marrow cells of green fluorescent protein (GFP) transgenic mice were transplanted into lethally irradiated C57BL/6 mice. Four weeks after bone marrow transplantation, spinal cord injury was produced by a static load (20 g, 5 min) at T8 level. G-CSF (200 μg/kg/day) was injected subcutaneously for 5 days. Immunohistochemistry for GFP and cell lineage markers was performed to evaluate G-CSF-mediated mobilization of bone marrow-derived cells into injured spinal cord. Hind limb locomotor recovery was assessed for 6 weeks. Immunohistochemistry revealed that G-CSF increased the number of GFP-positive cells in injured spinal cord, indicating that bone marrow-derived cells were mobilized and migrated into injured spinal cord. The numbers of double positive cells for GFP and glial markers were larger in the G-CSF treated mice than in the control mice. Luxol Fast Blue staining revealed that G-CSF promoted white matter sparing. G-CSF treated mice showed significant recovery of hind limb function compared to that of the control mice. In conclusion, G-CSF showed efficacy for spinal cord injury treatment through mobilization of bone marrow-derived cells.

1. Introduction

Due to recent advances in stem cell biology, the efficacy of cell therapy for central nervous system disorders, including spinal cord injury, has been reported. Amongst various types of cells, bone marrow-derived stem cells, which include hematopoietic stem cells (HSC) and bone marrow stromal cells (BMSC), also called mesenchymal stem cells (Bacigalupo, 2004; Herzog et al.,

* *Corresponding author.* Fax: +81 43 226 2116.
E-mail address: m-koda@bb.em-net.ne.jp (M. Koda).

0006-8993/$ – see front matter © 2007 Elsevier B.V. All rights reserved.
doi:10.1016/j.brainres.2007.02.058

2003), are candidates for cell therapy of spinal cord injury, because they can be transplanted autologously. Indeed, transplantation of HSC promotes functional recovery after compression-induced spinal cord injury in mice, as we reported previously (Koshizuka et al., 2004; Koda et al., 2005), and transplantation of BMSC significantly improves hind limb function after spinal cord injury in mice and rats (Chopp et al., 2000; Hofstetter et al., 2002; Wu et al., 2003). These lines of evidence show the potential of bone marrow-derived stem cells to restore injured spinal cord tissue and to promote functional recovery.

Granulocyte colony-stimulating factor (G-CSF) is widely known as a cytokine that induces survival, proliferation and differentiation of cells of the neutrophil lineage (Nicola et al., 1983; Roberts, 2005). Further, G-CSF can mobilize bone marrow cells into peripheral blood, an action used clinically for patients with leukocytopenia and for donors of peripheral blood-derived HSCs for transplantation (Jansen et al., 2005). Bone marrow-derived stem cells mobilized by G-CSF may have the potential to migrate into and repair various injured tissues. For example, G-CSF has been shown to mobilize bone marrow-derived stem cells to repair the ischemic myocardium (Orlic et al., 2001; Kawada et al., 2004). As for the central nervous system, bone marrow cells mobilized by G-CSF migrate into, survive and express a neural phenotype in normal brain (Corti et al., 2002a), spinal cord and dorsal root ganglia (Corti et al., 2002b). Moreover, G-CSF mobilized bone marrow cells into the ischemic brain and promoted functional recovery (Kawada et al., 2006). The influence of G-CSF-mediated mobilization of bone marrow-derived stem cells on the injured spinal cord remains to be elucidated.

Here we showed that G-CSF promoted the mobilization and migration of bone marrow cells into the spinal cord, the restoration of damaged spinal cord tissue and the recovery of hind limb function.

2. Results

Mice tolerated the irradiation and bone marrow transplantation well. FACS analysis showed that approximately 80% of the whole bone marrow cells were positive for GFP 4 weeks after bone marrow transplantation, indicating that GFP Tg-derived bone marrow cells survived and reconstituted hematopoiesis in grafted mice (not shown).

At first, we analyzed GFP fluorescence to detect bone marrow-derived cells in the intact spinal cord. The average number of GFP-positive cells was 33.6 (16–46) per section in the PBS group and 40.3 (18–61) per section in the G-CSF group (Fig. 1D). GFP-positive cells were located mainly in the white matter and subpial zone (Figs. 1A–C). There was no significant difference between the numbers of GFP-positive cells in the PBS and G-CSF groups (Fig. 1D).

Twenty-four hours after injury, GFP-positive cells had accumulated in the lesion epicenter. Most of the GFP-positive cells in the lesioned site were round, and the remaining were spindle-shaped (Figs. 2A, D). There was no significant difference between the number of GFP-positive cells in the SCI+PBS and SCI+G-CSF groups (352.4±24.2 in the SCI+PBS group and 331.7±23.6 in the SCI+G-CSF group, Fig. 2F). Next, we performed immunohistochemistry for cell-specific markers to elucidate the phenotype of GFP-positive cells in the injured spinal cord. Twenty-four hours after injury, GFP-positive

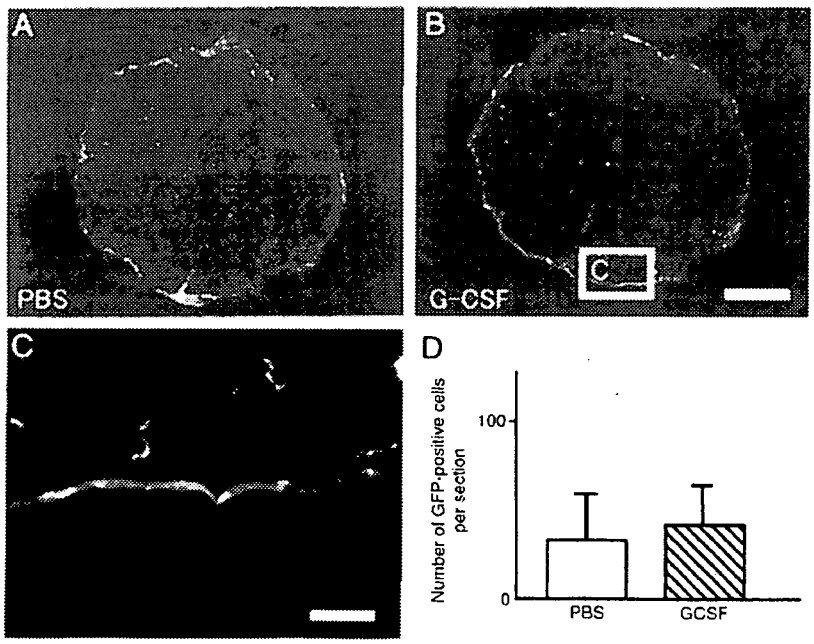

Fig. 1 – Immunohistochemistry for GFP in normal spinal cord after PBS (A) or G-CSF (B) injection. (C) is the higher-magnification view indicated as a box in (B). There was no significant difference in the number of GFP-positive cells between the PBS and G-CSF groups (D). GFP-positive cells were located in the white matter and subpial zone (C). Bars=500 μm (A, B) and 30 μm (C). Values are mean±S.E.M. (D).

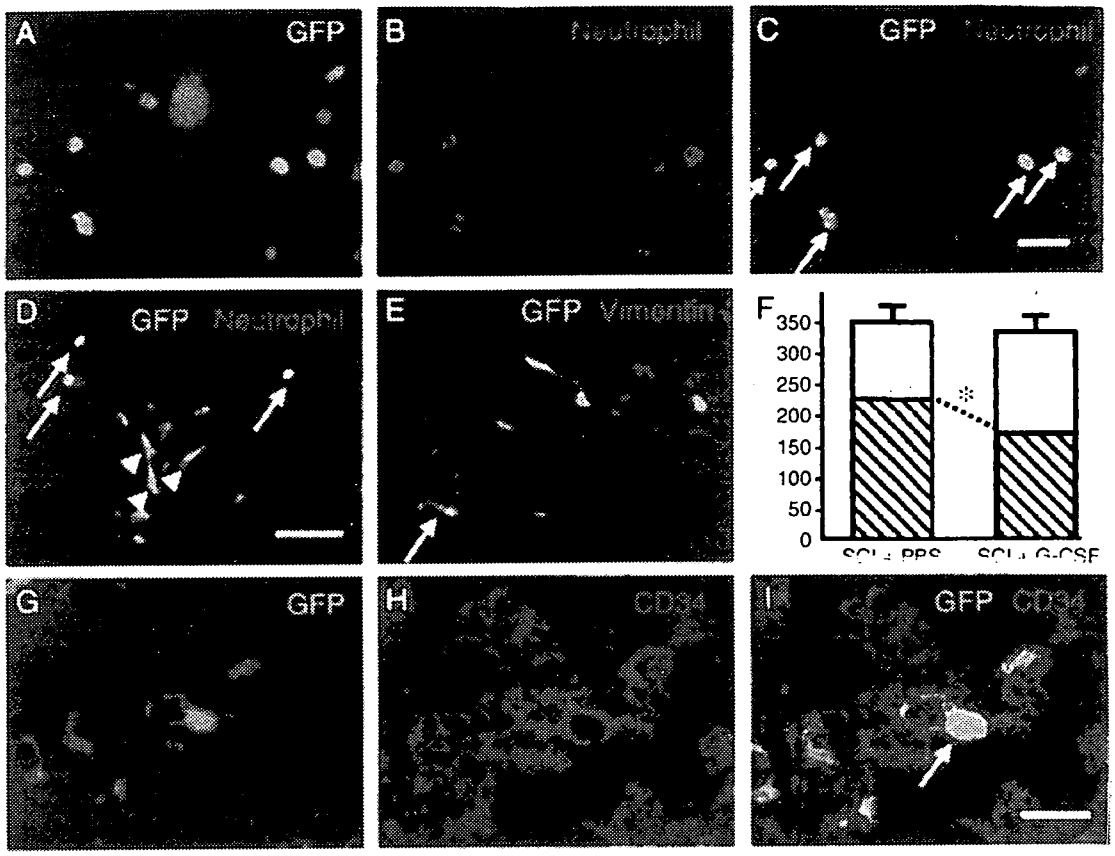

Fig. 2 – Immunohistochemistry for GFP and cell-specific markers in the acute phase of spinal cord injury. Near the lesion epicenter, GFP-positive round cells were also positive for neutrophil antigen (A–C, D, arrows). GFP-positive spindle-shaped cells negative for neutrophil antigen were observed (D, arrowheads). Some of the GFP-positive spindle-shaped cells were positive for vimentin, a marker for cells of the mesenchymal lineage (E, arrow). There was no significant difference in the number of GFP-positive cells between the SCI+PBS and SCI+G-CSF groups (F). The number of GFP- and neutrophil-double-positive cells was smaller in the SCI+G-CSF group than in the SCI+PBS group (F, hatched column, $p<0.05$). In the SCI+G-CSF group, GFP- and CD34-double-positive cells were detected near the lesion epicenter (G–I, arrow). Bars = 50 μm (A–C), 100 μm (D, E) and 30 μm (G–I).

round cells in the lesion epicenter were positive for neutrophil antigen (Figs. 2A–C, arrows). The number of cells double-positive for GFP and neutrophil antigen was smaller in the SCI+G-CSF group than that in the SCI+PBS group (Fig. 2F, hatched column). GFP-positive spindle-shaped cells were negative for neutrophil antigen (Fig. 2D, arrowheads). Some of the GFP-positive spindle-shaped cells were positive for vimentin, a marker for cells of the mesenchymal lineage (Fig.

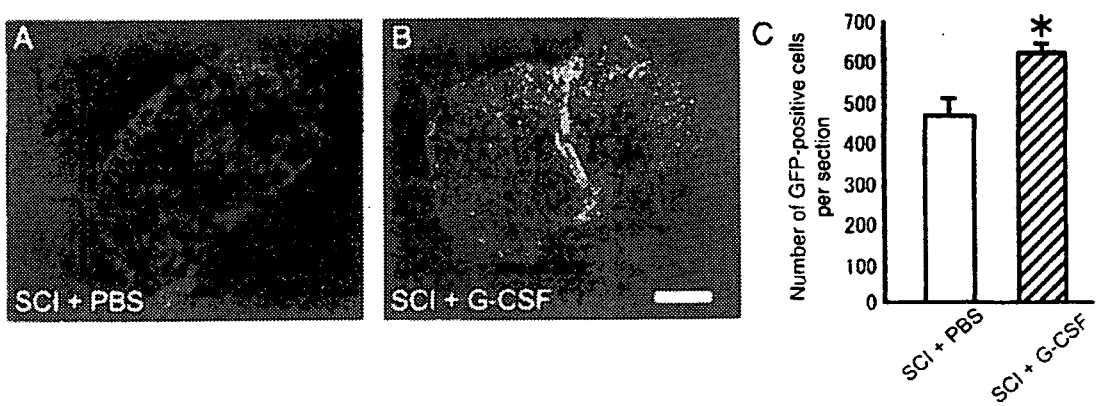

Fig. 3 – Immunohistochemistry for GFP in the chronic phase of spinal cord injury (A: the SCI+PBS group, B: the SCI+G-CSF group). The number of GFP-positive cells was larger in the SCI+G-CSF group (C, hatched column) than that in the SCI+PBS group (C, open column). Bar = 500 μm (A, B). Values are mean ± S.E.M. and *$p<0.05$ (C).

2E, arrow). No cells were double-positive for GFP and a neural lineage marker in the injured spinal cord in both the SCI+PBS and SCI+G-CSF groups 24 h after injury (not shown).

To confirm G-CSF-mediated mobilization of bone marrow-derived hematopoietic stem cells, we performed immunohistochemistry for CD34 one week after injury. In the SCI+G-CSF group, GFP- and CD34-double-positive cells were detected near the lesion epicenter (Figs. 2G–I, arrow).

Six weeks after injury, there were many GFP-positive round cells in the lesioned site and cells with some processes in the white matter (Figs. 3A, B). The number of GFP-positive cells in the SCI+G-CSF group was significantly larger than that in the SCI+PBS group 6 weeks after injury (449.0±28.5 in the SCI+PBS group and 610.3±21.9 in the SCI+G-CSF group, $p<0.003$, Fig. 3C). Most of the GFP-positive round cells in the lesioned site were positive for Mac-1, a marker for activated microglia/macrophages (Figs. 4A–C). The number of cells double-positive for GFP and Mac-1 was larger in the SCI+G-CSF group (392.6±44.0; Fig. 5A, hatched column) than that in the SCI+PBS group (338.6±36.4; Fig. 5A, open column). In the white matter, some of the GFP-positive cells were also positive APC (Figs. 4D–F, arrow), whereas there were no GFP- and nestin-double-

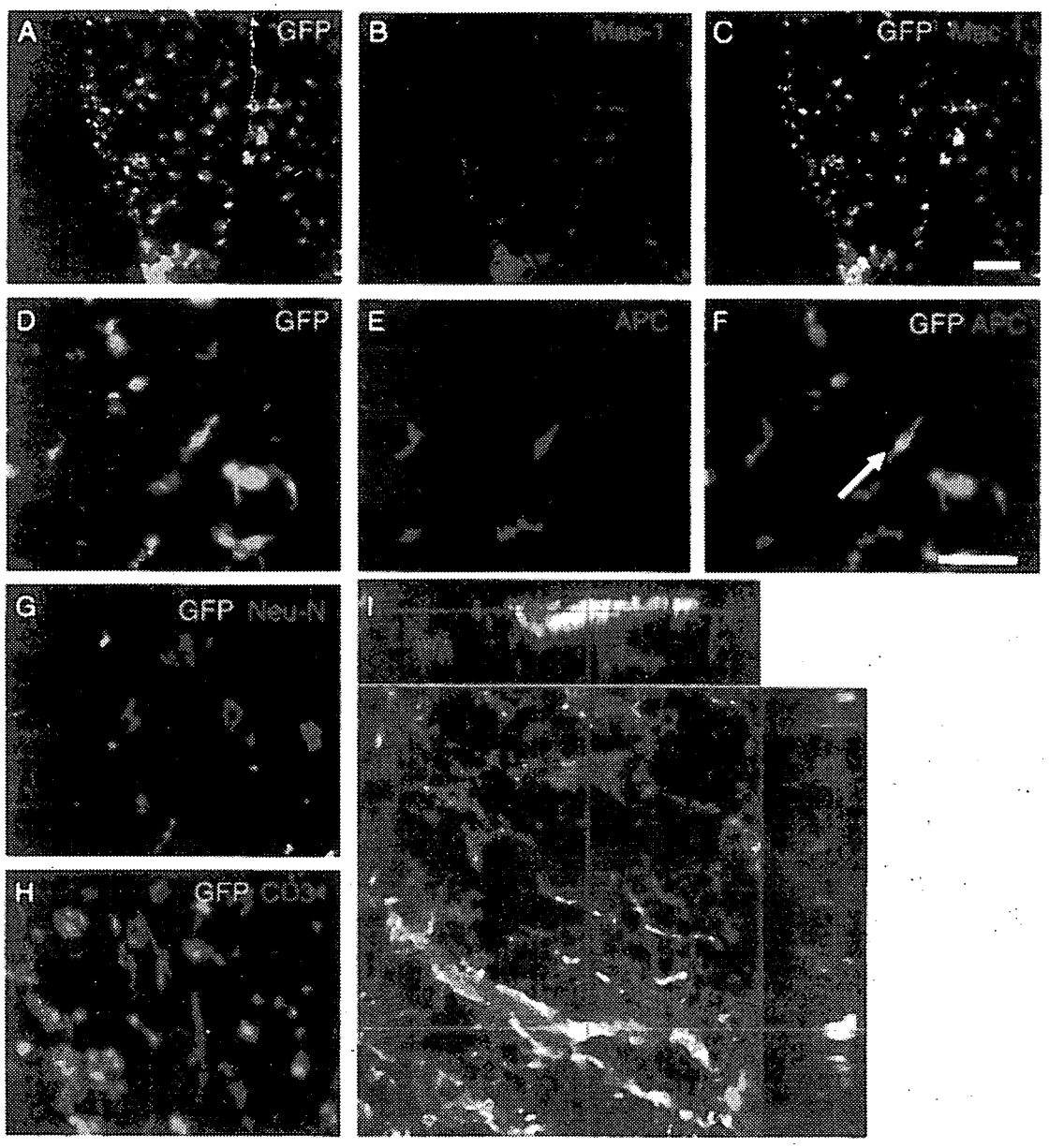

Fig. 4 – Double-immunofluorescence study for GFP and cell-specific markers in the SCI+G-CSF group 6 weeks after injury. Double-positive cells for GFP and Mac-1 (marker for macrophages/microglia; A–C), GFP and GFAP (marker for astrocytes; D–F, arrow), GFP and APC (marker for oligodendrocytes; D–F, arrow), whereas no GFP- and Neu-N (marker for neurons; G) or GFP- and CD-31 (marker for endothelial cells; H)-double-positive cells were observed. Three-dimensional reconstruction of confocal image of double immunofluorescent staining for GFP and GFAP revealed co-localization of GFP and GFAP (I). Bars = 100 μm (A–C) and 50 μm (D–R).

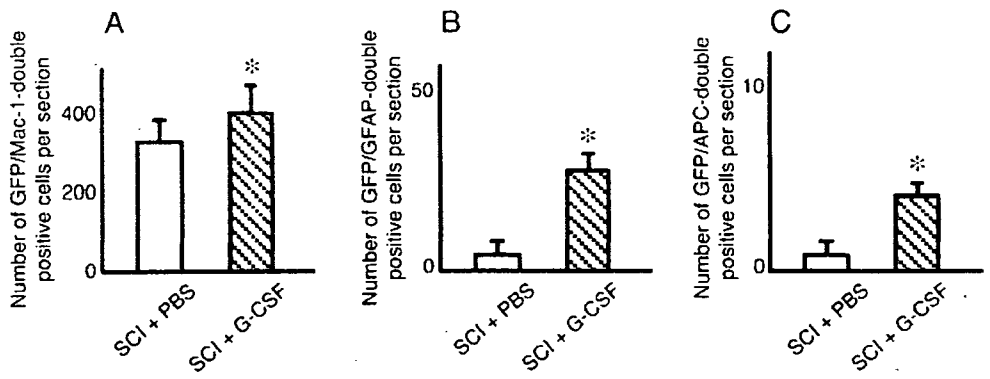

Fig. 5 – Quantitative analysis of double-positive cells for GFP and cell-specific markers 6 weeks after injury. The numbers of double-positive cells for GFP and Mac-1 (A), GFP and GFAP (B), GFP and APC (C) and GFP and nestin (D) were significantly larger in the SCI+G-CSG group than that in the SCI+PBS group. Values are mean±S.E.M. *$p<0.05$.

positive cells (not shown), GFP- and Neu-N-double-positive cells (Fig. 4G) nor GFP- and CD-31-double-positive cells (Fig. 4I) were detected. Three-dimensional reconstruction of confocal image of double immunofluorescent staining for GFP and GFAP revealed co-localization of GFP and GFAP (Fig. 4I).

The numbers of GFP- and GFAP-double-positive cells (SCI+PBS: 0.6±0.4, SCI+G-CSF: 36.0±4.2) and GFP- and APC-double-positive cells (SCI+PBS: 0.6±0.3, SCI+G-CSF: 3.6±1.6) were larger in the SCI+G-CSF group (Figs. 5B, C, hatched columns, $p<0.05$) than in the SCI+PBS group (Figs. 5B, C, open columns).

To assess spinal cord tissue restoration, we performed luxol fast blue (LFB) staining. The average area of LFB-positive spared white matter was significantly larger in the SCI+G-CSF group than that in the SCI+PBS group (Fig. 6), indicating that G-CSF promoted restoration of spinal cord tissue.

Finally, we assessed the recovery of hind limb function using the motor function scale (Farooque et al., 2001), in which the maximum hind limb motor function scale is 13. All mice had a score of 13 before surgery, and the score dropped to 0 immediately after the spinal cord injury. Significant recovery of hind limb function was observed in mice from the SCI+G-CSF group (Fig. 6A, square) 4 weeks ($p<0.05$), 5 weeks and 6 weeks after injury ($p<0.01$) compared with the SCI+PBS group (Fig. 7A, circle). The average recovery score in the SCI+G-CSF group 6 weeks after injury was 4.7, indicating rhythmic bilateral hind limb stepping without weight bearing, whereas the average score in the SCI+PBS group was 3.1, indicating obvious bilateral hind limb motion without rhythmic stepping (Fig. 7B). Two mice in the SCI+G-CSF group showed the highest recovery score 6, indicating weight-bearing ability of hind limbs with abnormal walking (external rotation of one or both limbs and/or hip instability). In the Farooque's motor function scale system we used in the current study, score above 6 indicates weight support ability, which has significant impact in clinical situation.

3. Discussion

In the present study, we demonstrated that G-CSF promoted the migration of bone marrow-derived cells into the lesioned spinal cord and accelerated the recovery of hind limb function.

G-CSF has the potential to mobilize bone marrow cells into the peripheral blood. It is well known that G-CSF can increase the concentration of HSCs in the peripheral blood to that equaling or exceeding the concentration in bone marrow (Jansen et al., 2005). In addition to HSCs, cells of other lineages in the bone marrow, including mesenchymal stem cells, can be mobilized into the peripheral blood by G-CSF (Kawada et al., 2004). In the present study, G-CSF increased the number of GFP-positive/neutrophil antigen-negative spindle-shaped cells in the lesioned site 24 h after injury and a part of that population of cells expressed vimentin, which is a marker for cells of the mesenchymal lineage. In addition, GFP- and CD34-

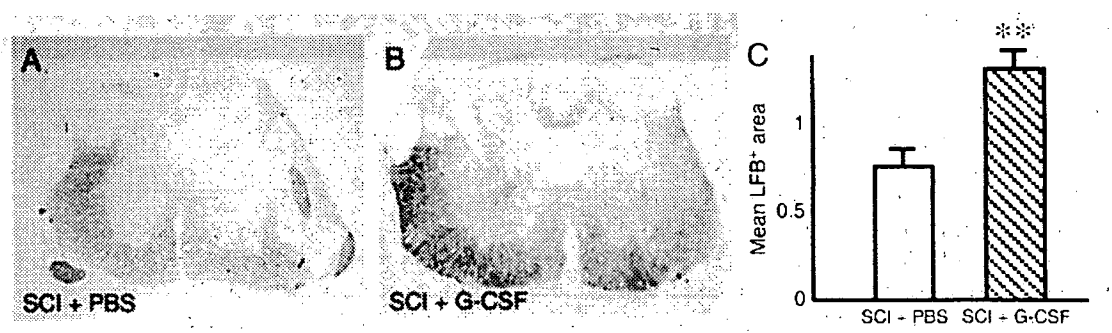

Fig. 6 – Luxol Fast Blue (LFB) staining to quantify white matter sparing. LFB-positive area in the SCI+G-CSF group (A) (C, hatched column) was significantly larger than that in the SCI+PBS group (B) (C, open column).

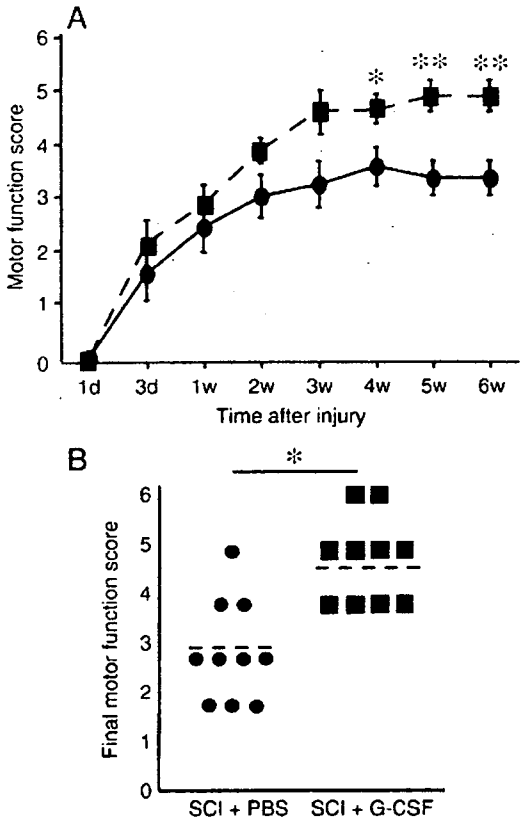

Fig. 7 – Hind limb functional assessment with the hind limb motor function scale (Farooque et al., 2001; Table 1). Time course of hind limb functional recovery (A) and comparison of final motor function score between the groups (B). Mice from the SCI+G-CSF group (square) showed significant recovery compared to mice from the SCI+PBS group (circle). Values are mean±S.E.M. *$p<0.05$, **$p<0.01$.

double-positive cells were detected near the lesion epicenter 1 week after injury. These findings may suggest that G-CSF promoted mobilization of bone marrow-derived stem cells, including HSCs and mesenchymal stem cells, both of which have the potential to restore damaged spinal cord tissue and to promote functional recovery, as we and others reported previously. The present results showed that G-CSF increased the number of bone marrow-derived cells in the injured spinal cord and promoted glial differentiation of bone marrow-derived cells in the chronic phase of spinal cord injury. These results may reflect the increase of G-CSF-mediated migration of bone marrow-derived stem cells into the lesioned spinal cord. In the present study, the differentiation of bone marrow-derived cells in the injured spinal cord was restricted to glial cells. It was reported that G-CSF promotes migration and differentiation into neurons of bone marrow-derived cells in normal and ischemic brain (Corti et al., 2002a; Kawada et al., 2006). A possible explanation is that the difference in the microenvironment between the brain and spinal cord and the difference between the ischemic and traumatic injury models cause a discrepancy between the results of the previous reports and the present results in the spinal cord injury model (Cao et al., 2001). Another possibility is that G-CSF modulated the environment in the injured spinal cord, including the cytokine expression profile (Zavala et al., 2002), resulting in enhancement of survival, proliferation and differentiation into cells of the neural lineage of bone marrow-derived stem cells that migrated into the lesioned site.

Hind limb function significantly improved in G-CSF-treated mice in the current study. Possible mechanisms of G-CSF-mediated functional recovery are as follows: 1) soluble factors secreted from bone marrow-derived stem cells that migrated into the lesioned spinal cord may ameliorate functional deficits. It is known that HSCs secrete growth factors that have neurotrophic properties (Takakura et al., 2000), and mesenchymal stem cells secrete interleukins and neurotrophic factors (Chopp and Li, 2002), by which HSCs and mesenchymal stem cells can contribute to the restoration of damaged central nervous tissue; 2) bone marrow-derived stem cells that were mobilized into the spinal cord by G-CSF into host spinal cord tissue. It has been reported that both HSCs (Cogle et al., 2004; Sigurjonsson et al., 2005) and mesenchymal stem cells (Tondreau et al., 2004) may have the potential to differentiate into neural cells, although the transdifferentiation of bone marrow cells is still controversial (Herzog et al., 2003). In addition to G-CSF-mediated differentiation into neural cells, G-CSF also increased the number of Mac-1-positive macrophages/microglia. Macrophages/microglia has the potential to scavenge cell debris around the lesioned site and to secrete neurotrophic factors, actions that can contribute to the restoration of the damaged spinal cord (Popovich, 2000; Bouhy et al., 2006).

Recently, it was reported that G-CSF- or GM-CSF-mediated mobilization of bone marrow-derived cells may promote spinal cord tissue restoration (Park et al., 2005 Urdzikova et al., 2006). However, their reports lack the direct evidence of bone marrow cell mobilization using bone marrow chimera mice. Moreover, in those reports, G-CSF or GM-CSF administration was initiated 1 week after injury, which is different from the present study. Further investigation is needed to elucidate the optimal time point of G-CSF-mediated bone marrow cell mobilization for spinal cord injury.

We also speculated that a direct neuroprotective effect of G-CSF may ameliorate functional deficits of spinal cord-injured mice. It is reported that G-CSF inhibits glutamate-induced neuronal death of cerebellar granule neurons *in vitro* and also inhibits ischemia-induced neuronal death in the rat brain *in vivo*, resulting in a decrease in infarction volume (Shäbitz et al., 2003; Schneider et al., 2005). These investigators also reported that the neuroprotective effect of G-CSF is mediated by the G-CSF receptor and its downstream signaling pathway. In the present study, there is a possibility that G-CSF may affect the spinal cord neurons and glial cells directly. Finally, suppression or modulation of cytokine expression by G-CSF may contribute to the restoration of the damaged spinal cord and functional recovery. It has been reported that G-CSF suppresses inflammatory cytokine expression of monocytes in vitro (Nishiki et al., 2004) and modulates inflammatory cytokine expression in experimental allergic encephalitis (Zavala et al., 2002). Inflammatory cytokines are thought to promote the progression of secondary injury in the acute phase of spinal cord injury. Further

investigation is needed to elucidate these mechanisms of action of G-CSF.

Regarding the clinical application of G-CSF for the treatment of spinal cord injury, G-CSF has some advantages over other treatments under investigation. First, G-CSF has already been approved as a safe drug, and it is widely used in clinics. Second, G-CSF-mediated mobilization of bone marrow-derived cells does not require injection of the cells directly into the lesioned spinal cord, thus avoiding additional trauma. Moreover, G-CSF-mediated mobilization of bone marrow-derived cells does not require harvesting and cultivation of any cells *in vitro*, resulting in the avoidance of associated risks including contamination, tumor formation, immunological rejection and ethical problems.

In conclusion, G-CSF promotes the migration of bone marrow-derived cells into the lesioned spinal cord and the recovery of hind limb function. The present results encourage the use of G-CSF to treat spinal cord injury, although further investigation is needed to advance G-CSF treatment for this clinical application.

4. Experimental procedure

4.1. *Bone marrow transplantation*

Bone marrow cells were collected from 8- to 12-week-old male green fluorescent protein transgenic mice (GFP Tg; Okabe et al., 1997). GFP Tg mice were euthanized with a pentobarbital overdose, and femurs and tibias were removed and placed in cold phosphate-buffered saline (PBS). After removal of the epiphyses of the femurs and tibias, the marrow was flushed out with PBS using a 26G needle attached to a syringe. A total of 6×10^6 bone marrow cells derived from GFP Tg mice were transplanted intravenously via the tail vein of lethally irradiated (10 Gy) female C57BL/6 mice (SLC, Hamamatsu, Japan). Four weeks after bone marrow transplantation, whole bone marrow cells were collected as mentioned above for fluorescence-activated cell-sorter (FACS) scanner analysis with FACScan (Becton Dickinson, San Jose, CA) to evaluate chimerism ($n=2$).

4.2. *Spinal cord injury and G-CSF treatment*

Four weeks after bone marrow transplantation, surgery and G-CSF treatment were performed. A total of 38 mice were used in the present study. Animals were divided into four groups, including spinal cord injury with G-CSF treatment (SCI+G-CSF group; $n=14$), spinal cord injury with vehicle control (SCI+PBS group; $n=14$), sham operation with G-CSF treatment (G-CSF group; $n=5$) and sham operation without G-CSF treatment (PBS group; $n=5$). Under halothane anesthesia, laminectomy was performed at the Th7–8 level, leaving the dura intact. The animals were then placed in a stereotaxic apparatus, and two adjustable forceps were applied to the spinous processes of both T6 and T9 to stabilize the spine. The dural tube was compressed with a steady load of 20 g for 5 min at the site of the Th7–8 laminectomy. The tip of the weight was a 1×2-mm rectangular plastic plate (Farooque et al., 2001). The mice were kept under a heating lamp until they regained consciousness. No pre- or post-operative antibiotics were given. Bladder function was observed during the first days after trauma for signs of urinary retention. Food and water were provided ad libitum before and after the experiments. The mice were kept in a temperature-controlled environment of 20 °C, and were exposed to alternate light and dark periods of 12 h. All animals were treated and cared for in accordance with the Chiba University School of Medicine guidelines pertaining to the treatment of experimental animals.

Immediately after injury, recombinant human G-CSF (200 μg/kg/day; kindly provided by Kirin Brewery Co. Ltd., Pharmatheutical Division, Tokyo, Japan) or vehicle alone (1% bovine serum albumin in PBS) was injected subcutaneously for 5 days in each group.

4.3. *Assessment of locomotor activity*

The functional recovery of hind limb of mice in the SCI+G-CSF ($n=10$) and SCI+PBS ($n=10$) groups was determined by measuring the hind limb motor function score as previously described by Farooque et al. (2001). Mice were allowed to move freely on the open field with rough surface for 5 min at each time tested. The hind limb movement of mice were videotaped and scored by two independent observers who were unaware of the treatment. Measurement of motor function was performed before surgery, 1 and 3 days and 1–6 weeks (once a week) after spinal cord injury. The scale ranged from 0 to 13, and scores were as shown in Table 1. In brief, score 0 means complete paralysis, scores 1–3 means movements of hind limbs without rhythmical stepping, scores 4 and 5 mean rhythmical motion of hind limbs without weight bearing ability, scores 6 and 7 mean weight bearing ability, scores 8–12

Table 1

Score	Criteria
0	No noticeable movements of the hind limbs.
1	Occasional, barely visible movements of any hind limb joint (hip, knee, or ankle).
2	Obvious movements of one or more joints in one hind limb but no forwards propulsive, stepping movements.
3	Obvious movements of one or more joints in both hind limbs but no forwards propulsive, stepping movements.
4	Stepping and forwards propulsive movement of one hind limb. No weight-bearing. Often external rotation of the hind limb.
5	Alternate stepping and forwards propulsive movements of both hind limbs but no weight-bearing ability. Often external rotation of hind limbs.
6	Weight-bearing ability of hind limbs but no normal walking (external rotation of one or both limbs and/or hip instability). The animals sweep one or both feet while walking (an obvious friction noise can be heard).
7	Weight-bearing ability of hind limbs, walks with a mild deficit (slight external rotation of one or both limbs and/or hip instability).
8	Normal movements except for reduced speed of walking.
9	Normal movements, ability to walk on a 2-cm wide bar.
10	Normal movements, ability to walk on a 1.5-cm wide bar.
11	Normal movements, ability to walk on a 1-cm wide bar.
12	Normal movements, ability to walk on a 7-mm wide bar.
13	Normal movements, ability to walk on a 5-mm wide bar.

means walking ability with increase of the hind limb gait width and score 13 means full recovery.

Mice in both the G-CSF and PBS groups were excluded from behavioral assessment, because they showed no apparent neurological deficit throughout the experimental period.

4.4. Tissue preparation

For histological evaluation, animals in all of the groups were perfused transcardially with 4% paraformaldehyde in PBS (pH 7.4) under pentobarbital anesthesia 1 day ($n=4$/group) and 6 weeks ($n=10$/group) after surgery. Three segments of spinal cords, including the lesion epicenter (T7–9) were removed and postfixed in the same fixative overnight, stored in 20% sucrose in PBS at 4 °C, and embedded in OCT compound (Sakura Finetechnical, Tokyo, Japan). The cryoprotected samples were frozen and kept at −80 °C until use. The samples were cut into serial 20-μm transverse sections with a cryostat and mounted onto poly-L-lysine-coated slides (Matsunami, Tokyo, Japan).

4.5. Histological assessment and immunohistochemistry

We performed luxol fast blue (LFB) staining to measure the area of spared white matter.

Immunohistochemistry was performed to identify the distribution and cell types of GFP-expressing bone marrow-derived cells, as previously described (Hashimoto et al., 2003; Kamada et al., 2005). The specificity of the staining procedures was controlled by omitting primary or secondary antibodies. The primary antibodies used were as follows: rat monoclonal anti-CD34 antibody (CD34, 1: 200, Acris Antibodies GmbH, Hiddenhausen, Germany), mouse monoclonal anti-neuronal nuclear antigen antibody (NeuN, 1:800, Chemicon Int., Temecula, CA) for neurons, mouse monoclonal anti-glial fibrillary acidic protein antibody (GFAP, 1:1600, Sigma) for astrocytes, mouse monoclonal anti-adenomatous polyposis coli antibody (APC, 1:800, Calbiochem, San Diego, CA) for oligodendrocytes, rat monoclonal anti-CD11b antibody (Mac-1, 1: 400, Serotec, Oxford, UK) for macrophages/microglia, rat monoclonal anti-neutrophil antibody (1:400, Serotec) for infiltrating neutrophils, mouse monoclonal anti-nestin (1:800, Chemicon Int.) for neural stem/progenitor cells and rat monoclonal anti-CD31 antibody (Pharmingen, San Jose, CA) for endothelial cells. The sections were reacted with cell-type marker antibodies overnight at 4 °C. After 3 10-min washes with PBS, the sections were reacted with Alexa 594-labeled anti-rabbit, anti-mouse or anti-rat IgG antibody (Molecular Probes) at room temperature for 1 h. The positive signals were observed by fluorescence microscope (ECLIPSE E600; Nikon, Tokyo, Japan). We also used Zeiss LSM 510 confocal laser scanning microscope to observe GFP- and GFAP-double-positive cells and GFP- and CD34-positive cells.

For quantitative analysis of the spared white matter area and the differentiation of bone marrow-derived cells that migrated into the spinal cord, every fifth 20-μm transverse sections (100 μm apart) were picked up from either 300–900 μm rostral or 300–900 μm caudal to the lesion epicenter. Sections near the lesion epicenter were excluded from histological and immunohistochemical assessment because the tissue destruction was too severe to perform quantitative analysis in that area. Six sections were taken from the spinal cords of mice from each group. The LFB-positive area was calculated using Scion Image computer analysis software (Scion Corporation, Frederick, MA). The sections were immunostained with antibodies to markers for each cell lineage, as described above. The numbers of double-positive cells and GFP-positive cells were summed.

4.6. Statistical analysis

GFP-positive cell count, double immunofluorescence study, LFB-positive area and the final motor function score were subjected to the Student's t-test. Motor function scores were subjected to Repeated Measures ANOVA followed by post hoc test using Scheffe's F test. Data are presented as mean values ± S.E. Values of $p<0.05$ were considered statistically significant.

Acknowledgments

We are grateful to Kirin Brewery Co. Ltd., Pharmatheutical Division for their kind gift of G-CSF. This work was supported by grants-in-aid for Scientific Research from the Ministry of Education, Science and Culture of Japan (16591473) and grant from the General Insurance Association of Japan.

REFERENCES

Bacigalupo, A., 2004. Mesenchymal stem cells and haematopoietic stem cell transplantation. Best Pract. Res., Clin. Haematol. 17, 387–399.

Bouhy, D., Malgrange, B., Multon, S., Poirrier, A.L., Scholtes, F., Schoenen, J., Franzen, R., 2006. Delayed GM-CSF treatment stimulates axonal regeneration and functional recovery in paraplegic rats via an increased BDNF expression by endogenous macrophages. FASEB J. 20, 1239–1241.

Cao, Q.L., Zhang, Y.P., Howard, R.M., Walters, W.M., Tsoulfas, P., Whittemore, S.R., 2001. Pluripotent stem cells engrafted into the normal or lesioned adult rat spinal cord are restricted to a glial lineage. Exp. Neurol. 167, 48–58.

Chopp, M., Li, Y., 2002. Treatment of neural injury with marrow stromal cells. Lancet Neurol. 1, 92–100.

Chopp, M., Zhang, X.H., Li, Y., 2000. Spinal cord injury in rat: treatment with bone marrow stromal cell transplantation. NeuroReport 11, 3001–3005.

Cogle, C.R., Yachnis, A.T., Laywell, E.D., Zander, D.S., Wingard, J.R., Steindler, D.A., Scott, E.W., 2004. Bone marrow transdifferentiation in brain after transplantation: a retrospective study. Lancet 363, 1432–1437.

Corti, S., Locatelli, F., Strazzer, S., Salani, S., Del Bo, R., Soligo, D., Bossolasco, P., Bersolin, N., Scarlato, G., Comi, C.P., 2002a. Modulated generation of neuronal cells from bone marrow by expansion and mobilization of circulating stem cells with in vivo cytokine treatment. Exp. Neurol. 177, 443–452.

Corti, S., Locatelli, F., Donadoni, C., Strazzers, S., Salani, S., Del Bo, R., Caccialanza, M., Bresolin, N., Scarlato, G., Comi, G.P., 2002b. Neuroectodermal and microglial differentiation of bone marrow cells in the mouse spinal cord and sensory ganglia. J. Neurosci. Res. 70, 721–733.

Farooque, M., Isaksson, J., Olsson, Y., 2001. Improved recovery after spinal cord injury in neuronal nitric oxide synthase-deficient mice but not in TNF-alpha-deficient mice. J. Neurotrauma 18, 105–114.

Hashimoto, M., Koda, M., Ino, H., Murakami, M., Yamazaki, M., Moriya, H., 2003. Upregulation of osteopontin expression in rat spinal cord microglia after traumatic injury. J. Neurotrauma 20, 287–296.

Herzog, E.L., Chai, L., Krause, D.S., 2003. Plasticity of marrow-derived stem cells. Blood 102, 3483–3493.

Hofstetter, C.P., Schwarz, E.J., Hess, D., Widenfalk, J., El Manira, A., Prockop, D.J., Olson, L., 2002. Marrow stromal cells form guiding strands in the injured spinal cord and promote recovery. Proc. Natl. Acad. Sci. U. S. A. 19, 2199–2204.

Jansen, J., Hanks, S., Thompson, J.M., Dugan, M.J., Akard, L.P., 2005. Transplantation of hematopoietic stem cells from the peripheral blood. J. Cell. Mol. Med. 9, 37–50.

Kamada, T., Koda, M., Dezawa, M., Yoshinaga, K., Hashimoto, M., Koshizuka, S., Nishio, Y., Moriya, H., Yamazaki, M., 2005. Transplantation of Schwann cells derived from bone marrow stromal cells promotes axonal regeneration and functional recovery after complete transection of adult rat spinal cord. J. Neuropathol. Exp. Neurol. 64, 37–45.

Kawada, H., Fujita, J., Kinjo, K., Matsuzaki, Y., Tsuma, M., Miyatake, H., Muguruma, Y., Tsuboi, K., Itabashi, Y., Ikeda, Y., Ogawa, S., Okano, H., Hotta, T., Ando, K., Fukuda, K., 2004. Nonhematopoietic mesenchymal stem cells can be mobilized and differentiate into cardiomyocytes after myocardial infarction. Blood 104, 3581–3587.

Kawada, H., Takizawa, S., Takanashi, T., Morita, Y., Fujita, J., Fukuda, K., Takagi, S., Okano, H., Ando, K., Hotta, T., 2006. Administration of hematopoietic cytokines in the subacute phase after cerebral infarction is effective for functional recovery facilitating proliferation of intrinsic neural stem/progenitor cells and transition of bone marrow-derived neuronal cells. Circulation 113, 701–710.

Koda, M., Okada, S., Nakayama, T., Koshizuka, S., Kamada, T., Nishio, Y., Someya, Y., Yoshinaga, K., Okawa, A., Moriya, H., Yamazaki, M., 2005. Hematopoietic stem cell and marrow stromal cell for spinal cord injury in mice. NeuroReport 16, 1763–1767.

Koshizuka, S., Okada, S., Okawa, A., Koda, M., Murasawa, M., Hashimoto, M., Kamada, T., Yoshinaga, K., Murakami, M., Moriya, H., Yamazaki, M., 2004. Transplanted hematopoietic stem cells from bone marrow differentiate into neural lineage cells and promote functional recovery after spinal cord injury in mice. J. Neuropathol. Exp. Neurol. 63, 64–72.

Nicola, N.A., Metcalf, D., Matsumoto, M., Johonson, G.R., 1983. Purification of a factor inducing differentiation in murine myelomonocytic leukemia cells. Identification as granulocyte colony-stimulating factor. J. Biol. Chem. 258, 9017–9023.

Nishiki, S., Hato, F., Kamata, N., Sakamoto, E., Hasegawa, T., Kimura-Eto, A., Hino, M., Kitagawa, S., 2004. Selective activation of STAT 3 in human monocytes stimulated by G-CSF: implication in inhibition of LPS-induced TNF-α production. Am. J. Physiol.: Cell Physiol. 286, 1302–1311.

Okabe, M., Ikawa, M., Kominami, K., Nakanishi, T., Nishimune, Y., 1997. 'Green mice' as a source of ubiquitous green cells. FEBS Lett. 407, 313–319.

Orlic, D., Kajstura, J., Chimenti, S., Limana, F., Jakoniuk, I., Quaini, F., Nadal-Ginard, B., Bodine, D.M., Leri, A., Anversa, P., 2001. Mobilized bone marrow cells repair the infarcted heart, improving function and survival. Proc. Natl. Acad. Sci. U. S. A. 98, 10344–10349.

Park, H.C., Shim, Y.S., Ha, Y., Yoon, S.H., Park, S.R., Choi, B.H., Park, H.S., 2005. Treatment of complete spinal cord injury patients by autologous bone marrow cell transplantation and administration of granulocyte–macrophage colony stimulating factor. Tissue Eng. 11, 913–922.

Popovich, P.G., 2000. Immunological regulation of neuronal degeneration and regeneration in the injured spinal cord. Prog. Brain Res. 128, 43–58.

Roberts, A.W., 2005. G-CSF: a key regulator of neutrophil production, but that's no all! Growth Factors 23, 33–41.

Schneider, A., Krüger, C., Steigleder, T., Weber, D., Pitzer, C., Laage, R., Aronowski, J., Maurer, M.H., Gassler, N., Mier, W., Hasselblatt, M., Kollmar, R., Schwab, S., Sommer, C., Bach, A., Kuhn, H.G., Shäbitz, W.R., 2005. The hematopoietic factor G-CSF is a neuronal ligand that counteracts programmed cell death and drives neurogenesis. J. Clin. Invest. 115, 2083–2098.

Shäbitz, W.R., Kollmar, R., Schwaninger, M., Juettler, E., Bardutzky, J., Schölzke, M.N., Sommer, C., Schwab, S., 2003. Neuroprotective effect of granulocyte colony-stimulating factor after focal cerebral ischemia. Stroke 34, 745–751.

Sigurjonsson, O.E., Perreault, M.C., Egeland, T., Glover, J.C., 2005. Adult human hematopoietic stem cells produce neurons efficiently in the regenerating chicken embryo spinal cord. Proc. Natl. Acad. Sci. U. S. A. 102, 5227–5232.

Takakura, N., Watanabe, T., Suenobu, S., Yamada, Y., Noda, T., Ito, Y., Satake, M., Suda, T., 2000. A role for hematopoietic stem cells in promoting angiogenesis. Cell 102, 199–209.

Tondreau, T., Lagneaux, L., Dejeneffe, M., Massy, M., Mortier, C., Delforge, A., Bron, D., 2004. Bone marrow-derived mesenchymal stem cells already express specific neural proteins before any differentiation. Differentiation 72, 319–326.

Urdzikova, L., Jendelova, P., Glogarova, K., Burian, M., Hajek, M., Sykova, E., 2006. Transplantation of bone marrow stem cells as well as mobilization by granulocyte-colony stimulating factor promotes recovery after spinal cord injury in rats. J. Neurotrauma 23, 1379–1391.

Wu, S., Suzuki, Y., Ejiri, Y., Noda, T., Bai, H., Kitada, M., Kataoka, K., Ohta, M., Chou, H., Ide, C., 2003. Bone marrow stromal cells enhance differentiation of cocultured neurosphere cells and promote regeneration of injured spinal cord. J. Neurosci. Res. 72, 343–351.

Zavala, F., Abad, S., Ezine, S., Taupin, V., Masson, A., Bach, J.F., 2002. G-CSF therapy of ongoing experimental allergic encephalomyelitis via chemokine- and cytokine-based immune deviation. J. Immunol. 168, 2011–2019.

J Neurosurg Spine 7:65–70, 2007

Traumatic C6–7 subluxation with anomalous course of vertebral arteries treated with pedicle screw/rod fixation

Case report

MASASHI YAMAZAKI, M.D., PH.D.,[1] TAKANA KOSHI, M.D.,[2] CHIKATO MANNOJI, M.D.,[1] AKIHIKO OKAWA, M.D., PH.D.,[1] AND MASAO KODA, M.D., PH.D.[1]

[1]Department of Orthopaedic Surgery, Chiba University Graduate School of Medicine; and [2]Department of Orthopaedic Surgery, Chiba Emergency Medical Center, Chiba, Japan

✓The authors report the case of a 62-year-old woman who suffered an accidental fall and complained of severe neck pain and right C-7 radiculopathy. A right C6–7 facet fracture–subluxation was diagnosed. Bone fragments impinged on the right C-7 nerve root at the neural foramen. The bilateral vertebral arteries (VAs) ascended at the anterior aspect of C-6 and C-5 and entered the transverse foramen at the C-4 level.

Based on findings of anomalous VAs, the authors applied a pedicle screw (PS)/rod system to effect surgical correction of the deformity. Intraoperatively, they successfully performed reduction of the subluxation, decompression of the impinged nerve root, and minimum single-segment fusion involving the placement of a PS/rod system. After surgery, the patient's neurological deficit dramatically improved and spinal fusion was completed without any loss of deformity correction.

Prior to surgery for cervical injuries, the possible presence of an abnormal VA course should be considered. Preoperative detection of anomalous VAs will affect decisions on the appropriate corrective surgery option in cases of cervical spine injuries. *(DOI: 10.3171/SPI-07/07/065)*

KEY WORDS • **cervical spine** • **pedicle screw** • **subluxation** • **vertebral artery anomaly**

SEVERAL surgical procedures have been attempted to treat fracture–subluxation occuring in the subaxial cervical spine, and the clinical outcomes of these operations have been reported.[3,9,10,13] To the best of our knowledge, however, there are no reports in which authors have described treatment for cervical subluxation associated with an anomalous VA course in the subaxial cervical spine. In the present report, we describe the surgical treatment of a patient with a unilateral fracture–subluxation at the right C6–7 facet joint associated with right C-7 radiculopathy and an abnormal entrance level of the bilateral VAs into the transverse foramen. In this patient, surgical treatment was successfully performed using a cervical PS/rod system.

Abbreviations used in this paper: CSF = cerebrospinal fluid; CT = computed tomography; MR = magnetic resonance; PICA = posterior inferior cerebellar artery; PS = pedicle screw; VA = vertebral artery.

Case Report

Examination. This 62-year-old woman suffered an accidental fall and sustained a blow to the head. When she arrived at our emergency center, she complained of severe neck pain and motor weakness in her right upper arm. She experienced decreased right-sided muscle power of finger and wrist extension (Grades 2/5 and 3/5, respectively). Moderate hypalgesia was present in the right C-7 dermatome. Her right upper-extremity triceps tendon reflex was decreased. There was no evidence of myelopathy.

Plain lateral radiography of the cervical spine revealed anterior translation of C-6 onto C-7 (Fig. 1A). No apparent congenital cervical skeletal anomaly was noted. An axial CT scan obtained at C6–7 showed a fractured right facet joint and bone fragments within the right neural foramen (Fig. 1B). A right parasagittal CT reconstruction demonstrated posterior translation of the fractured C-7 vertebra's superior facet forming a perched facet of the right C6–7 segment (Fig. 1C). In addition, bone fragments from the C-

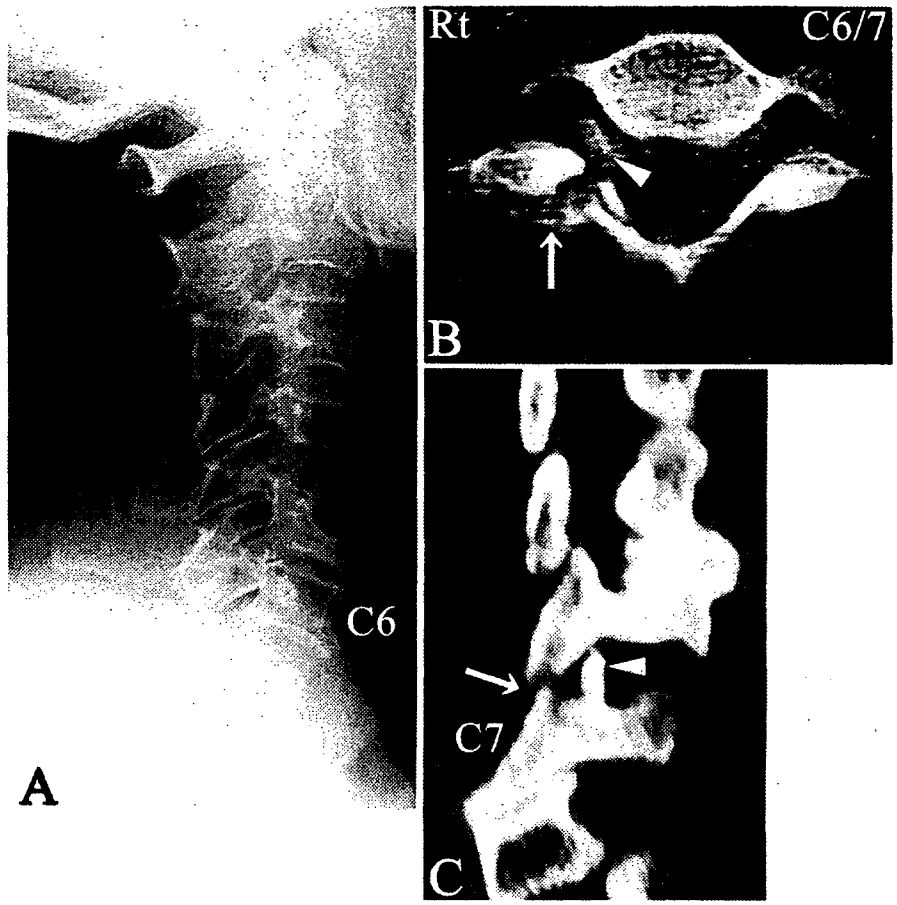

FIG. 1. Preoperative imaging studies. A: Plain lateral radiograph showing anterior translation of the C-6 vertebra relative to the C-7 vertebra. B: Axial CT scan obtained at the C6–7 level demonstrating a fractured right facet joint *(arrow)* and bone fragments in the right neural foramen *(arrowhead)*. C: Right parasagittal CT reconstruction revealing a fractured perched C6–7 facet joint *(arrow)* and bone fragments that migrated into the right C6–7 foramen *(arrowhead)*.

7 facet joint had migrated to the right C6–7 foramen (Fig. 1C). A left parasagittal CT reconstruction showed normal structures of the left facet joints, indicating a unilateral C6–7 fracture–subluxation. Both T1- and T2-weighted midsagittal MR imaging revealed mild anterior and posterior compression of the C6–7 cord, but indication of traumatic disc herniation was absent.

An axial CT scan at the C-1 level showed that the size of the transverse foramen on the left side was smaller than that on the right side (Fig. 2). In addition, axial CT images of the subaxial cervical spine showed that the bilateral transverse foramina at C-5 and C-6 were smaller compared with those at C-3 and C-4 (Fig. 2). These CT findings indicated the presence of an abnormal course of bilateral VAs in the cervical spine. To analyze the VA anomalies, we first performed MR angiography but its findings were unclear because of the artifact caused by the patient's false teeth. In addition, the precision of the CT scanner in our emergency center was insufficient to perform CT angiography. Thus, in the present case, we used conventional catheter angiography to evaluate the details of the VA anomalies.

Selective left VA angiograms demonstrated that the left VA ascended at the anterior aspect of the C-6 and C-5 vertebrae (Figs. 3A *[arrowheads]* and 4) and entered the transverse foramen at C-4 (Figs. 3A and B *[arrows]* and 4). In addition, the left VA did not run through the C-1 transverse foramen after emerging from the C-2 transverse foramen but, rather, entered the spinal canal at the caudal aspect of C-1 (Figs. 3A and B *[double arrows]* and 4), shifting directly to the left PICA (Fig. 3A and B *[asterisks]*). The right VA angiogram demonstrated that the right VA ascended at the anterior aspect of C-5 and C-6 (Figs. 3C *[arrowheads]* and 4) and entered the transverse foramen at C-4 (Figs. 3C and D *[arrows]* and 4), as was observed in the left VA. Regarding the upper cervical region, the course of the right VA was normal after emerging from the C-2 transverse foramen, entering into the spinal canal at the cranial aspect of C-1 (Figs. 3C and D *[double arrows]* and 4).

Preoperative Planning. Because fractured bone fragments were present within the neural foramen, we did not perform a closed reduction. We believed that the risk of the bone fragments' impingement of the right C-7 nerve root would be reinforced at the time of reposition. Thus, we planned a surgical treatment that consisted of decompression of the impinged root, reduction of the subluxation, and spinal fusion.

Based on the radiological findings of the abnormal course of the bilateral VAs, we believed that there would be

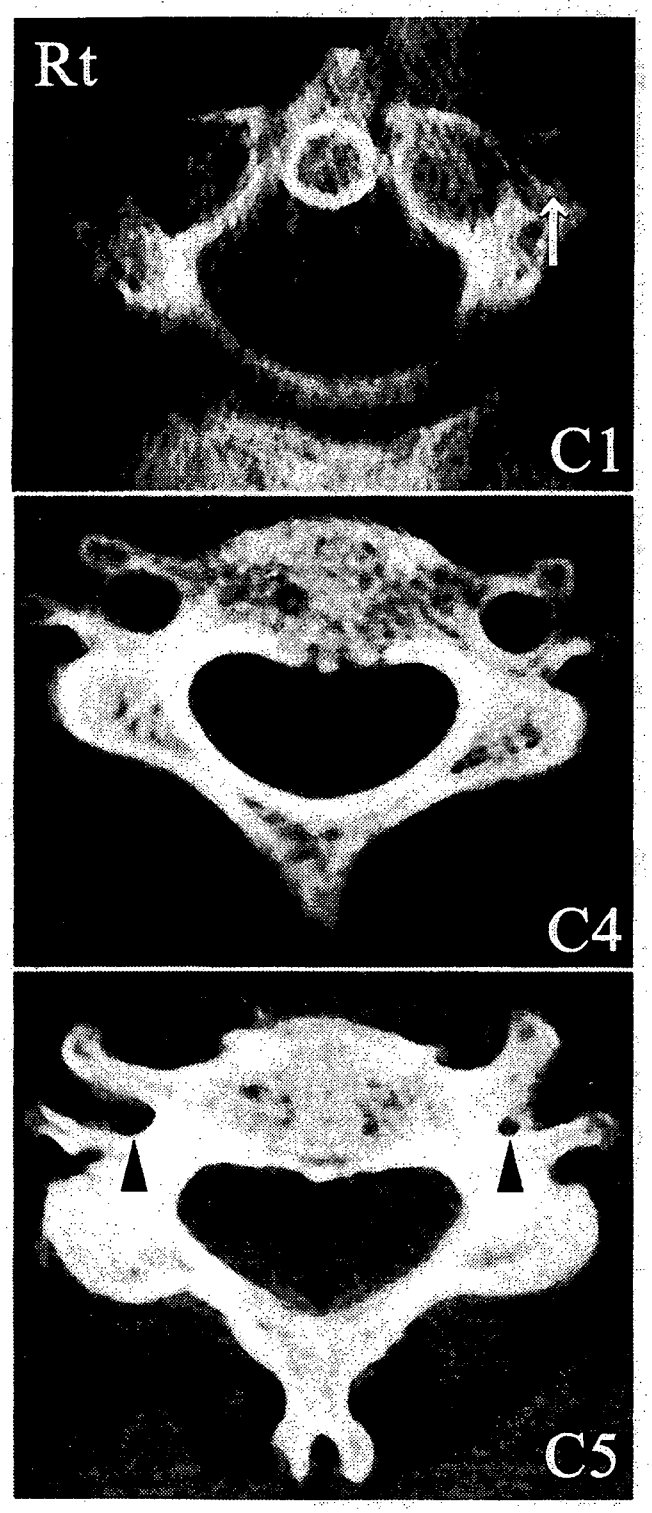

FIG. 2. Axial CT scans acquired at the C-1 *(upper)*, C-4 *(center)*, and C-5 *(lower)* levels showing that the size of the transverse foramen was smaller at C-1 on the left side *(arrow)* and at C-5 on both the left and right sides *(arrowheads)*.

an increased risk of VA injury when following an anterior approach to the C6–7 region because the VAs were unprotected by the transverse process. In contrast, the risk of VA injury due to PS insertion at C6–7 was decreased. Thus, we performed a one-stage posterior surgery that consisted of unroofing of the right C-7 nerve root, repositioning of the deformity, and spinal fusion in which a PS/rod system was placed.[1]

Operation. The patient was placed prone. On exposing the C-6 and C-7 laminae and bilateral facet joints, we observed disruption of the C6–7 ligamentum flavum and joint capsule bilaterally. At this stage, we observed CSF leaking from the right C6–7 interlaminar space. The right C-7 superior facet was fractured and translated posteriorly, forming the perched C6–7 facet on the right side. Segmental mobility at C6–7 was increased compared with the adjacent C5–6 and C7–T1 segments. We inserted PSs at C-6 and C-7 bilaterally. To improve the safety and accuracy of the screw insertion, we performed pedicle probing under lateral radiographic imaging. In addition, we used an angled device that had been developed in our laboratory (unpublished data). After insertion of the probe, we resected the caudal portion of the C-6 lamina, the cranial portion of the C-7 lamina, and the C6–7 facet on the right side. During this process, we found bone fragments compressing the lateral portion of the dura mater and the C-7 nerve root on the right side. After removal of the bone fragments, we found a small dural tear at the dura–nerve root sheath transitional region. We confirmed that CSF leaked through this tear.

After unroofing the right C-7 nerve root, we fixed 4.75-mm-diameter Isola rods to the screws on both sides. Tightening the locking nuts resulted in complete repositioning of the C6–7 subluxation. A strut was harvested from the left iliac crest and grafted onto both sides of the C6–7 spinous process by using an interspinous process wiring technique. We placed a free fat graft on the dural tear and sprayed fibrin gel over the fat tissue to shield the right C6–7 space and prevent CSF leakage.

Postoperative Course. Postoperative cervical radiographs showed the PS/rod system had completely reduced the subluxation deformity (Fig. 5A). Axial CT scanning demonstrated proper positioning of the PSs (Fig. 5B) and extensive unroofing of the right C-7 nerve root (Fig. 5B *arrow*). On the day following surgery, the patient experienced relief of her neck pain. She gradually recovered muscle power in her right upper arm, which returned to normal 10 months after the surgery. Follow-up radiographs acquired 1 year after surgery demonstrated complete spinal fusion at C6–7 without any loss of spinal correction (Fig. 5A). At the final follow-up examination 2 years after surgery, the patient had no neurological deficits, did not suffer of any neck pain, and had no restriction in neck motion.

Discussion

Bruneau et al.[4] analyzed the courses of VAs in the subaxial cervical spine in 250 patients and found that 93% of the arteries ran a normal course and entered the C-6 transverse foramen. In the other 7% the entrance level of the VA was abnormal as follows: at C-3 in 0.2%, C-4 in 1.0%, C-5 in 5%, and C-7 in 0.8% of cases. Thirty-one (12.4%) of the 250 patients harbored a unilateral anomaly of the VA entrance level, and only two patients (0.8%) had bilateral VA anomalies. In the present case, the bilateral VAs entered

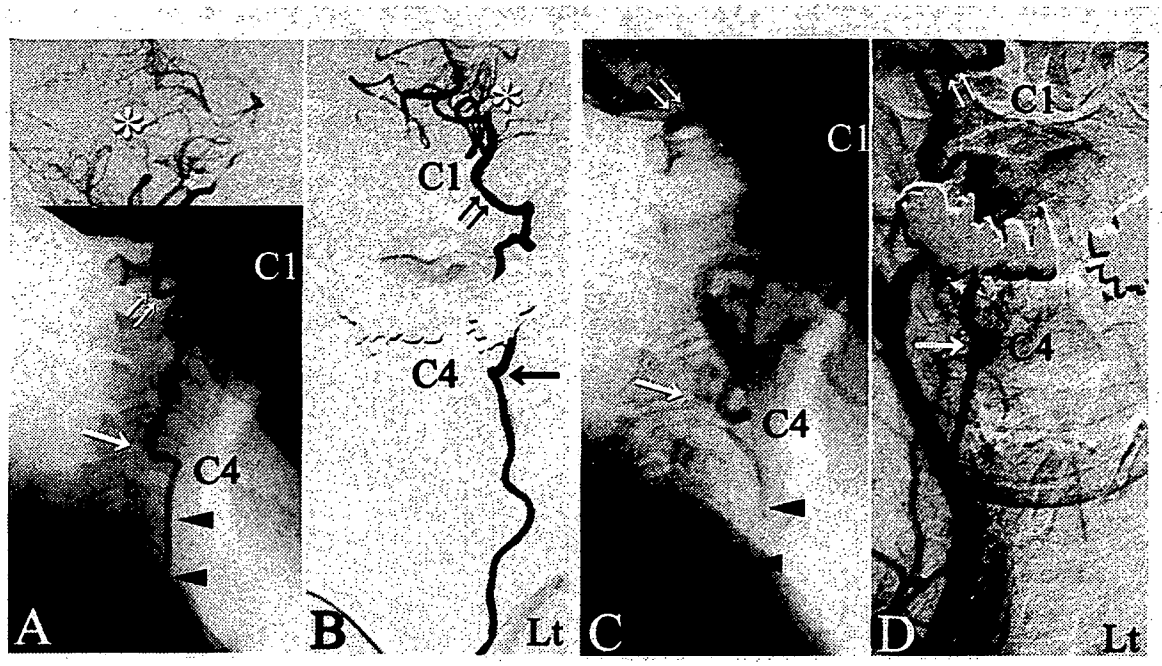

FIG. 3. Lateral (A and C) and anteroposterior (B and D) angiograms with selective contrast of the left (A and B) and right (C and D) VAs. The left VA ascends at the anterior aspect of C-6 and C-5 (*arrowheads*, A) and enters the transverse foramen at C-4 (*arrows*, A and B). The left VA does not run through the C-1 transverse foramen after emerging from the C-2 transverse foramen but enters the spinal canal at the caudal aspect of C-1 (*double arrows*, A and B), shifting directly to the left PICA (*asterisks*, A and B). The right VA ascends at the anterior aspect of C-6 and C-5 (*arrowheads*, C) and enters the transverse foramen at C-4 (*arrows*, C and D). The right VA runs a normal course after emerging from the C-2 transverse foramen and enters into the spinal canal at the cranial aspect of C-1 (*double arrows*, C and D). The top portion of the image in A and the entirety of the images in B and C are subtraction images. In C and D, the right VA is not selectively contrasted, but other arteries, including the carotid artery, are contrasted simultaneously.

into the transverse foramen at the C-4 level, indicating a rare anatomical variation of the VA entrance level.

Tokuda et al.[15] analyzed VA courses at the craniovertebral junction in 300 patients and reported two patients (0.67%) in whom the PICA originated from the VA between C-1 and C-2 and entered into the spinal canal from the caudal side of C-1. This was supplementarily examined by Sato et al.,[12] who found that the incidence of such VA anomalies was 0.36%. In the present case, the same type of VA anomaly described by Tokuda et al. was present in our patient on the left side. To the best of our knowledge, there have been no reports of cases in which different types of VA anomalies were simultaneously present at the craniovertebral junction and the subaxial cervical spine, as was observed in the present case.

For detecting VA anomalies, there have been several analytical methods including catheter-based angiography, MR angiography, and 3D CT angiography.[16] Among these, MR angiography and 3D CT angiography are less invasive than catheter angiography. In addition, 3D CT angiography has the additional advantages that it can depict VA images more precisely and reconstruct the image from a voluntary direction, delineating the VA and the circumferential osseous tissue simultaneously.[16] Despite these benefits of MR angiography and 3D CT angiography, we used catheter angiography in the present case because the MR angiograms were unclear due to artifact, and the precision of our CT scanner was insufficient to perform 3D CT angiography.

Previous reports of cases on the clinical outcome of radiculopathy associated with unilateral cervical spine injury in which radiculopathy persisted after treatment showed that persistence of radiculopathy was more frequent when the cervical injury was treated conservatively and/or the reduction of the displaced facet was insufficient.[9,10] In the present case, impingement of the right C-7 nerve root was caused by bone fragments derived from the fractured facets. We recognized the importance of anatomical reduc-

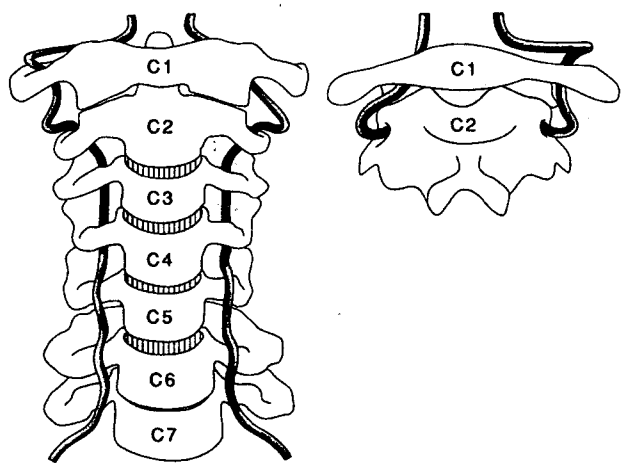

FIG. 4. Schematic drawings of the anomalous courses of bilateral VAs seen anteriorly *(left)* and posteriorly *(right)*.

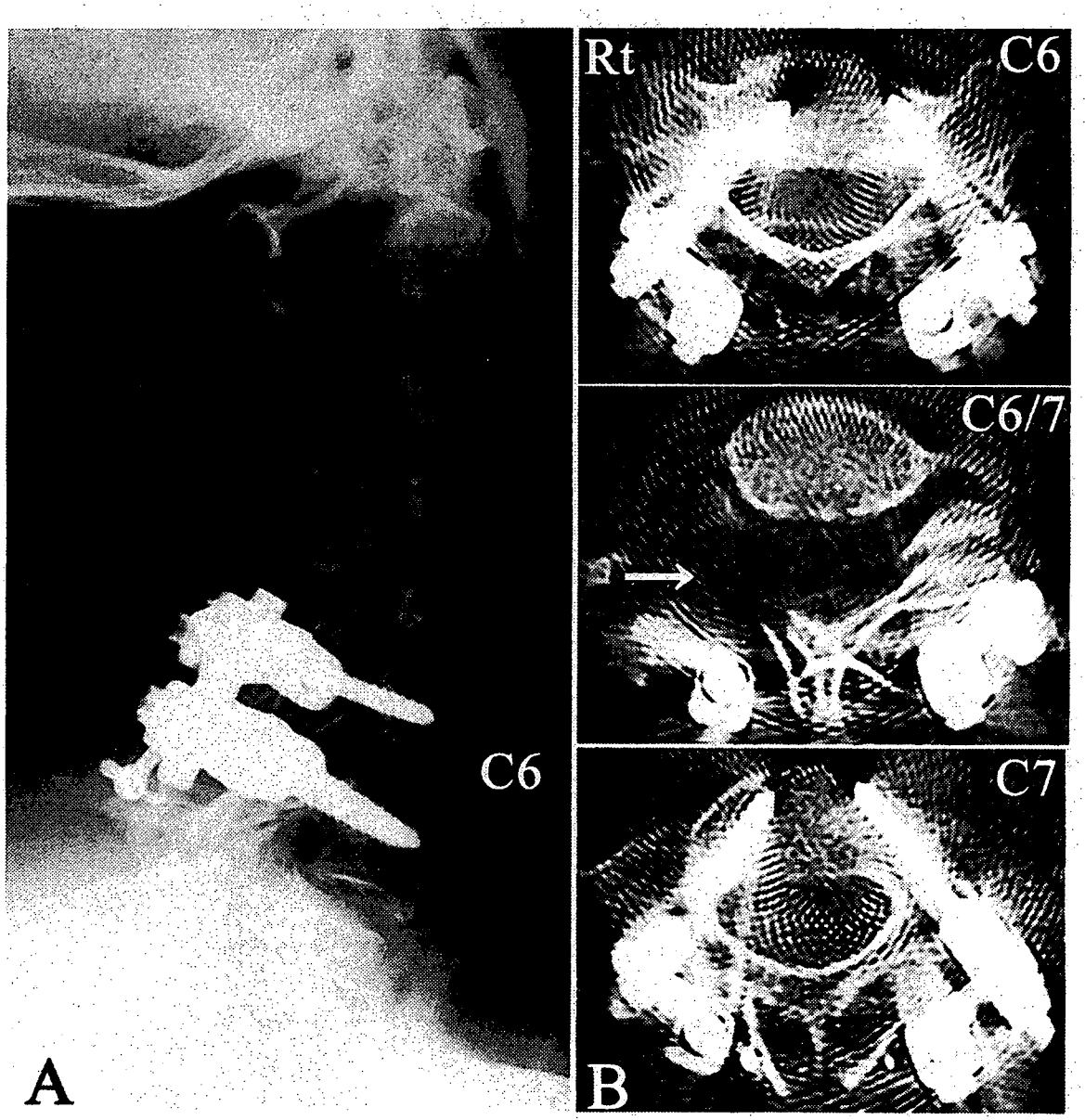

FIG. 5. Follow-up imaging studies. A: Plain lateral radiograph obtained 1 year after surgery showing complete reduction of the C6–7 subluxation and spinal fusion after application of the PS/rod system. B: Axial CT scans obtained at the C6 *(upper)*, C6–7 *(center)*, and C-7 *(lower)* levels taken 3 weeks after surgery demonstrating proper insertion and positioning of the PSs and extensive unroofing of the right C-7 nerve root *(arrow)*.

tion of the subluxation, appropriate decompression of the damaged nerve root, and stabilization of the injured segment of vertebrae.

The authors of previous reports have described using open reduction for unilateral cervical injury performed via anterior or posterior approaches.[3,9,13] There have also been reports of intraoperative VA injury during anterior cervical fusion.[5,14] In the present case, the bilateral VAs ascended at the anterior aspect of the vertebrae and remained unprotected by the transverse processes at the C5–7 levels. Thus, the risk of VA injury in anterior surgery would be much higher than that in cases of normal VA anatomy, and we decided that a posterior approach would be more appropriate in this case.

With regard to posterior surgeries for the reduction and stabilization of unilateral cervical injuries, other investigators have described the application of a lateral mass plate system,[9,13] which provided satisfactory results in many of these cases; however, late-developing kyphosis occurred in some patients in whom lateral mass plate systems were used.[9] During surgical planning in the present case, questions arose on whether fixation with lateral mass screws could stabilize the spine in minimum, single-segment (C6–7) surgery. In addition, our intention to unroof the right C-7 nerve root indicated that only a limited area would be available for the insertion of right C-6 lateral mass screws. In light of these treatment factors, we concluded that utilization of lateral mass screws for the anchors would have required us to perform no less than a two-level C5–7 fusion.

Authors of biomechanical studies on the cervical spine have reported that PSs have greater resistance to pullout forces than lateral mass screws[8] and are superior for the correction of cervical injury. The insertion of PSs at the C3–6 levels, however, poses a potential risk of VA injury that may result in serious complications.[11] In the present case, the bilateral VAs did not run through the transverse foramina but were located at the anterior aspect of the C-6 vertebral body. Thus, the intraoperative risk of VA injury with the insertion of C-6 PSs was extremely low. When the superior, inferior, or medial wall of the pedicle is perforated by the screw, a risk of nerve root injury exists. Abumi et al.[2] have reported that two of 669 cervical PSs caused nerve root injury, but other investigators have shown that the incidence of nerve root complication associated with lateral mass screws is not necessarily lower than that of PSs.[6,7] We therefore decided to apply a PS fixation system containing a rigid constrained screw/rod connection.[1] In using this system, we were able to execute a perfect anatomical reduction of the displaced cervical spine. Although extensive unroofing of the right C-7 nerve root was necessary, we achieved stabilization of the spine with minimum single-segment (C6–7) surgery.

Conclusions

Before undertaking surgery in cases of cervical spine injury, the possible presence of an anomalous VA course should be taken into account. A preoperative imaging demonstration of the detailed VA course will affect decisions regarding the appropriate surgical procedure for corrective surgery of cervical injuries.

References

1. Abumi K, Kaneda K, Shono Y, Fujiya M: One-stage posterior decompression and reconstruction of the cervical spine by using pedicle screw fixation systems. **J Neurosurg 90 (1 Suppl):**19–26, 1999
2. Abumi K, Shono Y, Ito M, Taneichi H, Kotani Y, Kaneda K: Complications of pedicle screw fixation in reconstructive surgery of the cervical spine. **Spine 25:**962–969, 2000
3. Beyer CA, Cabanela ME, Berquist TH: Unilateral facet dislocations and fracture-dislocations of the cervical spine. **J Bone Joint Surg Br 73:**977–981, 1991
4. Bruneau M, Cornelius JF, Marneffe V, Triffaux M, George B: Anatomical variations of the V2 segment of the vertebral artery. **Neurosurgery 59 (1 Suppl):**ONS20–ONS24, 2006
5. Golfinos JG, Dickman CA, Zabramski JM, Sonntag VK, Spetzler RF: Repair of vertebral artery injury during anterior cervical decompression. **Spine 19:**2552–2556, 1994
6. Graham AW, Swank ML, Kinard RE, Lowery GL, Dials BE: Posterior cervical arthrodesis and stabilization with a lateral mass plate. Clinical and computed tomographic evaluation of lateral mass screw placement and associated complications. **Spine 21:** 323–329, 1996
7. Heller JG, Silcox DH III, Sutterlin CE III: Complications of posterior cervical plating. **Spine 20:**2442–2448, 1995
8. Jones EL, Heller JG, Silcox DH, Hutton WC: Cervical pedicle screws versus lateral mass screws. Anatomic feasibility and biomechanical comparison. **Spine 22:**977–982, 1997
9. Lifeso RM, Colucci MA: Anterior fusion for rotationally unstable cervical spine fractures. **Spine 25:**2028–2034, 2000
10. Rorabeck CH, Rock MG, Hawkins RJ, Bourne RB: Unilateral facet dislocation of the cervical spine: an analysis of the results of treatment in 26 patients. **Spine 12:**23–27, 1987
11. Roy-Camille R, Mazel C, Saillant G, Benazet JP: Rationale and techniques of internal fixation in trauma of the cervical spine, in Errico T, Bauer RD, Waugh WT (eds): **Spine Trauma.** Philadelphia: JB Lippincott, 1991, pp 163–169
12. Sato K, Watanabe T, Yoshimoto T, Kameyama M: Magnetic resonance imaging of C2 segmental type of vertebral artery. **Surg Neurol 41:**45–51, 1994
13. Shapiro S, Snyder W, Kaufman K, Abel T: Outcome of 51 cases of unilateral locked cervical facets: interspinous braided cable for lateral mass plate fusion compared with interspinous wire and facet wiring with iliac crest. **J Neurosurg 91 (1 Suppl):**19–24, 1999
14. Smith MD, Emery SE, Dudley A, Murray KJ, Leventhal M: Vertebral artery injury during anterior decompression of the cervical spine. A retrospective review of ten patients. **J Bone Joint Surg Br 75:**410–415, 1993
15. Tokuda K, Miyasaka K, Abe H, Abe S, Takei H, Sugimoto S, et al: Anomalous atlantoaxial portions of vertebral and posterior inferior cerebellar arteries. **Neuroradiology 27:**410–413, 1985
16. Yamazaki M, Koda M, Aramomi MA, Hashimoto M, Masaki Y, Okawa A: Anomalous vertebral artery at the extraosseous and intraosseous regions of the craniovertebral junction: analysis by three-dimensional computed tomography angiography. **Spine 30:** 2452–2457, 2005

Manuscript submitted November 18, 2006.
Accepted March 26, 2007.

Address reprint requests to: Masashi Yamazaki, M.D., Ph.D., Department of Orthopaedic Surgery, Chiba University Graduate School of Medicine, 1-8-1 Inohana, Chuo-ku, Chiba 260-8677, Japan. email: masashiy@faculty.chiba-u.jp.

SPINE Volume 32, Number 18, pp E532–E536

Usefulness of 3-Dimensional Full-Scale Modeling for Preoperative Simulation of Surgery in a Patient With Old Unilateral Cervical Fracture-Dislocation

Masashi Yamazaki, MD, PhD, Akihiko Okawa, MD, PhD, Tsutomu Akazawa, MD, PhD, and Masao Koda, MD, PhD

Study Design. Case report.

Objective. We describe the usefulness of 3-dimensional full-scale modeling for preoperative simulation of surgery in a patient with old cervical fracture-dislocation.

Summary of Background Data. Many different surgical procedures have been used in the treatment of unilateral cervical fracture-dislocation. However, consistent protocols and procedures for the surgical correction of old fracture-dislocations associated with nerve root lesions have not been established.

Methods. Two months after an automobile accident, a 50-year-old man developed symptoms of left C5 palsy. Four months after the accident, he was diagnosed with a fracture-dislocation at left C4–C5 facet with impingement of the left C5 root at the neural foramen. In addition, his left vertebral artery was completely occluded. Spontaneous bony fusion had progressed around the left facet and the anterior aspect of the vertebrae at C4–C5. Before surgery, a 3-dimensional full-scale model in the patient's cervical spine was made in order to simulate the planned surgical reconstruction.

Results. Through this simulation, we were able to accurately evaluate the deformed bony structures around the fractured C4–C5 facet. During the actual surgery, all the planned procedures were successfully achieved, including anterior release, insertion of pedicle screws at left C4 and C5, unroofing of the left C5 root, reduction of the displaced facet with the pedicle screw-rod system, and spinal fusion at C4–C5. After surgery, the patient's left C5 palsy was dramatically relieved and the spinal fusion went on to successful healing.

Conclusion. The surgical simulation made possible by the 3-dimensional full-scale model appeared to simplify the surgical procedure and may enhance the safety of the complex spinal reconstruction.

Key words: dislocation, cervical spine, radiculopathy, pedicle screw, 3-dimensional full-scale model. **Spine 2007; 32:E532–E536**

As part of the treatment of unilateral fracture-dislocations of the middle-lower cervical spine, several surgical procedures have been described for reduction of displaced facets and vertebrae, decompression of damaged neural tissues, and stabilization of the cervical spine.[1–8] To the best of our knowledge, however, no report has discussed the treatment for old unilateral cervical fracture-dislocation associated with late onset radiculopathy and occlusion of the vertebral artery (VA).

In the present report, we describe our experience with surgical treatment of a patient who had an old unilateral fracture-dislocation at left C4–C5 associated with late onset C5 palsy and occlusion of the left VA. Before the surgery, we created a 3-dimensional (3D) full-scale model of the patient's cervical spine from computed tomography (CT) data.[9,10] Using the model, we performed a simulation of the corrective surgery with a pedicle screw-rod system. This simulation greatly assisted us in accurately and safely accomplishing the planned procedures.

■ Case Reports

Clinical Profile. A 50-year-old man was involved in an automobile accident while he was driving a car. During his transport to a hospital emergency room, he complained of severe neck pain, but no sensory and motor deficit was observed in his upper and lower extremities. Radiographs taken at the initial hospital at the time of his arrival did not appear to show any abnormal findings in his cervical spine, although they visualized only down to the midportion of the C4 vertebral body and therefore missed a C4–C5 dislocation. The patient failed to follow up with continued medical care, and only returned back when he developed symptoms of an acute left C5 palsy 2 months after the accident. Radiologic examination 3 months after the accident identified the C4–C5 dislocation. The patient was referred to our hospital for treatment of the C4–C5 dislocation.

On admission to our hospital 4 months after the accident, the patient complained of severe neck pain and numbness of the lateral side of his left upper arm. His shoulder abduction muscle power was decreased to 2/5, and elbow flexion was slightly decreased to 4/5 at the left side. He exhibited sensory loss in the left C5 dermatome area and had a decreased biceps tendon reflex in his left upper extremity. He showed no findings of myelopathy.

Radiologic Findings. A plain lateral radiograph of the cervical spine showed anterior displacement of the C4 vertebra relative to the C5 vertebra (Figure 1A). A midsagittal reconstruction image of the CT myelogram (Figure 1B, upper) showed that the spinal cord was slightly compressed anteriorly by the posterior-superior edge of the C5 vertebra. An axial image of the CT myelogram at the C4–C5 level showed that the left

From the Department of Orthopaedic Surgery, Chiba University Graduate School of Medicine, Inohana, Chuo-ku, Chiba, Japan.
Acknowledgment date: October 30, 2006. First revision date: February 25, 2007. Second revision date: March 8, 2007. Acceptance date: March 13, 2007.
The device(s)/drug(s) that is/are the subject of this manuscript is/are not FDA-approved for this indication and is/are not commercially available in the United States.
No funds were received in support of this work. No benefits in any form have been or will be received from a commercial party related directly or indirectly to the subject of this manuscript.
Address correspondence to Masashi Yamazaki, MD, PhD, Department of Orthopaedic Surgery, Chiba University Graduate School of Medicine, 1-8-1 Inohana, Chuo-ku, Chiba 260-8677, Japan; E-mail: masashiy@faculty.chiba-u.jp

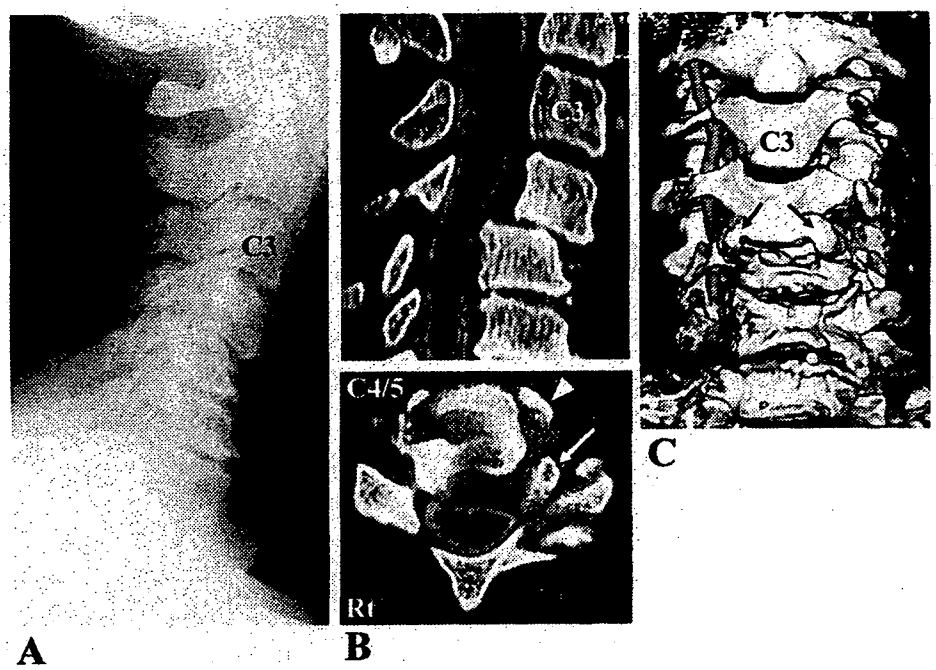

Figure 1. A preoperative plain lateral radiograph (**A**) shows anterior displacement of the C4 vertebra. A midsagittal reconstruction image (**B**, upper) of the computed tomography (CT) myelogram shows anterior compression of the spinal cord by the C5 vertebra. An axial image of the CT myelogram at C4–C5 (B, lower) shows bone fragments within the left C4–C5 foramen (arrow) and at the anterior aspect of the C4–C5 vertebrae (arrowhead). Anterior view of 3-dimensional CT angiography (**C**) shows occlusion of left vertebral artery (VA) and bony bridges over the C4–C5 vertebrae (arrows).

C4–C5 foramen contained bone fragments originating from the fractured left C4–C5 facet (Figure 1B, lower, arrow), indicating impingement of the left C5 root at the left C4–C5 foramen. The image also showed bone fragments at the anterior aspect of the C4–C5 vertebrae, indicating a partial vertebral body fracture (Figure 1B, lower, arrowhead). An axial image of the CT myelogram at the C5 level showed a fracture of the left transverse process of C5. Anterior view of the 3D CT angiography (Figure 1C), in conjunction with magnetic resonance (MR) angiography findings, revealed occlusion of the left VA. The images also showed bony bridges over the C4 and C5 vertebrae (Figure 1C, arrows).

Surgical Simulation. The surgical procedure we initially planned consisted of partial bone excision of the deformed fused left C4–C5 facet, unroofing of the left C5 root, correction of the deformity, and spinal fusion with a pedicle screw-rod system.[11] To evaluate the details of the anatomic structure of the patient's cervical spine, we used a rapid prototyping technique to manufacture a 3D full-scale model of his cervical spine from his CT data (Figure 2A, B). Our model clearly showed the deformed C4–C5 facet.

Before the actual operation, we performed a simulation of our planned surgery on the model. First, we inserted pedicle screws at C4 and C5 on the left side (Figure 2A, B). Using the model, we then determined the area of bone excision required to achieve posterior release of the left C4–C5 facet and unroofing of the left C5 root (Figure 2C). This simulation clearly demonstrated that the left C4–C5 facet was remarkably thickened and that spontaneous bone union had progressed not only at the fractured facet (Figure 2C, upper) but also at the anterior aspect of the C4–C5 vertebrae (Figure 2C, lower, arrow). Based on this information, we concluded that successful reduction of the locked facet would require bone excision through both anterior and posterior approaches.

Operation. The first stage of the actual surgery was an anterior release. We resected the bony bridges between the C4 and

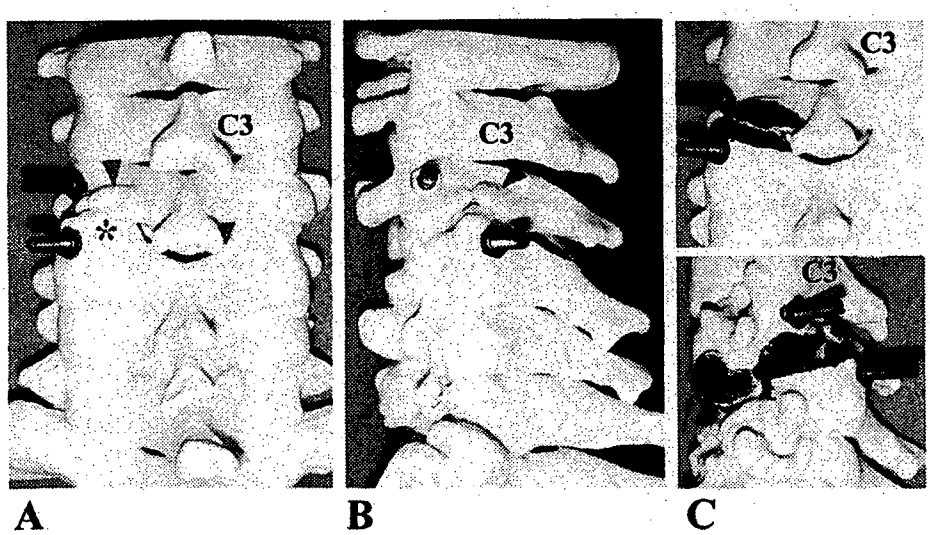

Figure 2. Posterior (**A**) and left lateral (**B**) views of the 3-dimensional full-scale model show the pedicle screws inserted at C4 and C5 on the left side. The fractured left C4 inferior facet (arrowhead) and posteriorly translated left C5 superior facet (asterisk) are indicated. Posterior (**C**, upper) and left anterior-lateral (C, lower) views of the model show the area marked with black ink where bone excision is planned. An arrow identifies a bony bridge over the C4–C5 vertebrae.

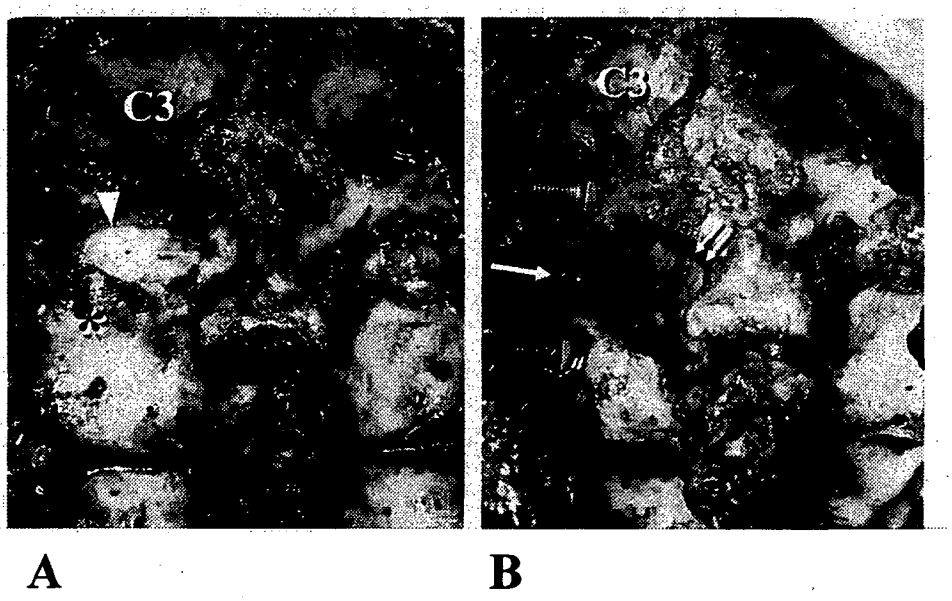

Figure 3. These 2 intraoperative photographs illustrate key moments of the actual surgery. **A**, Exposure of the C4 and C5 laminae and the left C4–C5 facets reveals a fractured left C4 inferior facet (arrowhead) and posterior translation of the left C5 superior facet (asterisk). **B**, Pedicle screws have been inserted at C4 and C5 on the left side; the left C5 root has been progressively unroofed until the lateral edge of the facet was reached (arrow). Double arrow indicates dura mater.

C5 vertebrae, excised the caudal portion of the C4 vertebra and the cranial portion of the C5 vertebra. We next excised the lateral wall of the C4 and C5 vertebrae until the left uncovertebral joint was completely removed. During this procedure, our 3D full-scale model was quite useful for detecting the deformation of the bony structure around the uncovertebral joint. After completing the anterior release, we inserted a disc interspace spreader and dilated the C4–C5 space. However, our reduction from the anterior direction was not successful.

We began the second stage of the surgery by repositioning the patient into a prone position. On exposure of the C4 and C5 laminae and bilateral facets, we observed a progressed bony union at the fracture site of the left C4–C5 facet (Figure 3A) and no mobility of the C4–C5 segment. We inserted pedicle screws at C4 and C5 on the left side. By looking at the 3D full-scale model intraoperatively, we were able to evaluate the anatomic landmarks of the displaced fractured facet of the left side in detail and to accurately determine the insertion points of the pedicle screws. After inserting the pedicle screws, we resected the caudal portion of the C4 lamina, the cranial portion of the C5 lamina, and the C4–C5 facet on the left side. During this process, we first located the dura mater (Figure 3B, double arrows) and then progressively unroofed the left C5 root until we reached the lateral edge of the facet (Figure 3B, arrow).

After completing the left C4–C5 facet resection, we performed a manual reduction of the dislocation. Even at this stage of the operation, however, we were not able to properly perform the reposition. We then installed a 4.75-mm diameter ISOLA rod to the screws. Tightening the locking nuts resulted in posterior translation of C4 vertebra and complete repositioning of C4 relative to C5. A strut bone was harvested from the iliac crest, and grafted onto the right side of the spinous process from C4–C5 using an interspinous process wiring technique.

For the third stage of this surgery, the patient was moved back into a supine position. Anterior intervertebral fusion from C4–C5 was performed using a tricortical strut bone from the iliac crest.

Postoperative Course. Postoperative cervical radiographs showed complete reduction of the dislocation with the pedicle screw and rod system. CT reconstruction images demonstrated extensive unroofing of the left C5 root (Figure 4B, C, arrow) and proper positioning of pedicle screws (Figure 4C).

On the day following surgery, the patient felt pain relief in his neck and left upper arm. Two days after surgery, he was able to elevate his left upper arm. Eleven months after surgery, his left upper arm muscle power had returned to normal. Follow-up radiographs taken 20 months after surgery showed complete spinal fusion at C4–C5 without any correction loss (Figure 4A). At this 20-month follow-up visit, the patient exhibited no neurologic deficits, did not complain of any pain in his neck and left upper arm, and had no restriction in his neck motion.

■ Discussion

Regarding the neurologic deficits associated with unilateral cervical dislocation/fracture-dislocation, previous studies found that the incidence of radiculopathy exceeded 60%.[2,8] Other reports also observed high incidences of radiculopathy in cervical injuries with similar pathologic conditions, including lateral mass/facet fracture[3] and unilateral lamina/facet fracture.[4] To the best of our knowledge, however, no report has described late onset C5 palsy associated with unilateral cervical fracture-dislocation, as was observed in the present case. In the present case, the source of impingement of left C5 root was probably bone fragments from the fractured facets. Presumably, the persistence of segmental mobility at C4–C5 after the injury enabled progressive migration of the bone fragments into the neural foramen, increasing the damage to the left C5 root.

When unilateral facet dislocation of the cervical spine was left in an unreduced position, it resulted in a mechanical malalignment that might cause increased incidence of late disc degeneration, late pain, or root entrapment.[2,7] As for the clinical outcome of radiculopathy associated with unilateral cervical spine injury, previous reports identified cases in which radiculopathy persisted

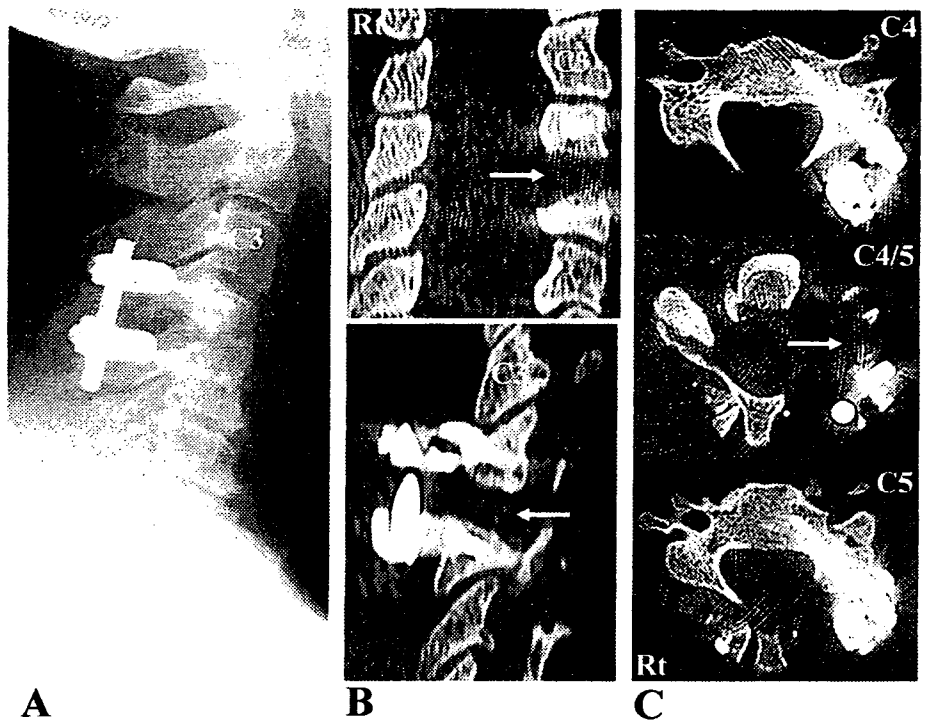

Figure 4. A plain lateral radiograph 1 year and 8 months after surgery (**A**) shows complete reduction of the C4–C5 dislocation and spinal fusion. Frontal (**B**, upper) and right parasagittal (B, lower) CT reconstruction images 1 week after surgery show successful unroofing of the left C5 root (arrow). Axial CT images at the C4, C4–C5, and C5 levels (**C**) show proper insertion and positioning of the pedicle screws and extensive unroofing of the left C5 root (arrow).

after the treatment.[4,7] Persistence of radiculopathy was more frequent when the cervical injury was treated conservatively and/or the reduction of the displaced facet was insufficient. These observations indicate the importance of incorporating anatomic reduction of the deformity, appropriate decompression of the damaged nerve root, and stabilization of the injured segment of vertebrae into the treatment of radiculopathy associated with unilateral cervical fracture-dislocation.

Previous reports have described the application of a lateral mass plating system for the reduction and stabilization of unilateral cervical dislocation/fracture-dislocation.[4,8] In many cases, this system provided satisfactory results. However, late-developing kyphosis occurred in some patients treated with lateral mass plate systems.[4] Previous biomechanical studies in the cervical spine have reported that pedicle screws have greater resistance to pull-out forces compared with lateral mass screws,[12] demonstrating the superiority of pedicle screws for the reduction of rigid transitional deformities of the cervical spine. In the present case, therefore, we selected a pedicle screw-rod system containing a rigid constrained screw-rod connection.[11] By using this system, we were able to achieve perfect anatomic reduction of the displaced cervical spine. Although we performed an extensive unroofing of the left C5 root, we achieved stabilization of the spine with a minimum single segment (C4–C5) surgery.

In the present case, since images of 3D CT angiography showed occlusion of left VA, injuring the remaining right VA during surgery could have resulted in serious complications due to consequent brainstem ischemia.[13] We therefore eliminated pedicle screw insertion into the right side during our surgery. Taneichi *et al* analyzed 11 patients with traumatically induced VA occlusion associated with cervical spine injuries and found that restoration of VA blood flow occurred after treatment in 3 of their 11 patients.[14] This study led us to insert pedicle screws carefully and accurately even on the VA-occluded side. In the present case, we conducted a surgical simulation of the pedicle screw insertion at C4–C5 and the anterior and posterior releases using the 3D full-scale model. Through the simulation, we could accurately evaluate the detailed bony structures of the deformed cervical vertebrae. Intraoperatively, the model facilitated our understanding of the anatomic landmarks around the facet joint, lateral mass, and osseous bridges over C4–C5 disc, thereby enabling us to successfully insert pedicle screws and accomplish the appropriate anterior and posterior releases during actual surgery.

■ Key Points

- We report a case of old fracture-dislocation at left C4–C5 facet, late-onset C5 palsy, and occlusion of the left vertebral artery.
- Reduction of the deformity, decompression of the impinged left C5 nerve root, and spinal fusion at C4–C5 were successfully performed using a pedicle screw-rod system.
- Surgical simulation using a 3D full-scale model simplified the surgical procedure and enhanced the safety of the complex spinal reconstruction for this patient.

References

1. Allred CD, Sledge JB. Irreducible dislocations of the cervical spine with a prolapsed disc: preliminary results from a treatment technique. *Spine* 2001; 26:1927–30.
2. Beyer CA, Cabanela ME, Berquist TH. Unilateral facet dislocations and fracture-dislocations of the cervical spine. *J Bone Joint Surg Br* 1991;73:977–81.
3. Kotani Y, Abumi K, Ito M, et al. Cervical spine injuries associated with lateral mass and facet joint fractures: new classification and surgical treatment with pedicle screw fixation. *Eur Spine J* 2005;14:69–77.
4. Lifeso RM, Colucci MA. Anterior fusion for rotationally unstable cervical spine fractures. *Spine* 2000;25:2028–34.
5. Ordonez BJ, Benzel EC, Naderi S, et al. Cervical facet dislocation: techniques for ventral reduction and stabilization. *J Neurosurg* 2000;92(suppl 1):18–23.
6. Payer M. Immediate open anterior reduction and antero-posterior fixation/fusion for bilateral cervical locked facets. *Acta Neurochir* 2005;147:509–13.
7. Rorabeck CH, Rock MG, Hawkins RJ, et al. Unilateral facet dislocation of the cervical spine: an analysis of the results of treatment in 26 patients. *Spine* 1987;12:23–7.
8. Shapiro S, Snyder W, Kaufman K, et al. Outcome of 51 cases of unilateral locked cervical facets: interspinous braided cable for lateral mass plate fusion compared with interspinous wire and facet wiring with iliac crest. *J Neurosurg* 1999;91(suppl 1):19–24.
9. Yamazaki M, Akazawa T, Koda M, et al. Surgical simulation of instrumented posterior occipitocervical fusion in a child with congenital skeletal anomaly: case report. *Spine* 2006;31:E590–4.
10. Yamazaki M, Akazawa T, Okawa A, et al. Usefulness of three-dimensional full-scale modeling of surgery for a giant cell tumor of the cervical spine. *Spinal Cord* 2007;45:250–3.
11. Abumi K, Kaneda K, Shono Y, et al. One-stage posterior decompression and reconstruction of the cervical spine by using pedicle screw fixation systems. *J Neurosurg* 1999;90(suppl 1):19–26.
12. Jones EL, Heller JG, Silcox DH, et al. Cervical pedicle screws versus lateral mass screws: anatomic feasibility and biomechanical comparison. *Spine* 1997;22:977–82.
13. Kim SH, Ahn YH, Cho KG. Poor surgical technique in cervical plating leading to vertebral artery injury and brain stem infarction: case report. *Surg Neurol* 2005;64:221–5.
14. Taneichi H, Suda K, Kajino T, et al. Traumatically induced vertebral artery occlusion associated with cervical spine injuries: prospective study using magnetic resonance angiography. *Spine* 2005;30:1955–62.